Czech University of Life Sciences Prague

Faculty of Engineering

Department of Material Science and Manufacturing Technology

ABRASIVE WEAR OF METAL MATRIX COMPOSITES

Diploma Thesis

Basudev Aryal

Supervisor

Assoc. Prof. Rostislav Choteborsky

Declaration

I hereby, declare that this thesis is my own work and effort and that it has not been submitted anywhere for any award. Where other sources of information have been used, they have been cited.

Basudev Aryal Prague, 06/04/2020

ABSTRACT

Abrasive wear is one of the most frequent and extensive wear an agricultural tool goes through a tool with high resistance to abrasive wear is preferred at the lowest cost possible. To meet the requirement and to produce the tools which last long and is cost effective, manufacturer considers the criteria such as required wear resistance, hardness and toughness. Agricultural tool wear resistance depends on the change of structure with the applied heat treatment, chemical composition used in the tool material, their hardenability and physical and mechanical of properties of the soil.

Materials were tested and evaluated for their abrasive wear resistance in the laboratory using the dry rubber wheel testing machine (ASTM G-95). To determine hardness of the material Vicker's hardness test was performed.

Microstructure of material's worn surfaces were inspected with the aid of microscope and the result shows that the materials possess higher wear resistance with increase in boron content which is in correlation with the materials hardness.

KEYWORDS

Abrasive wear, Heat treatment, Composite, Dry rubber wheel test, Vickers's hardness test

Acknowledgements

I would like to thank all individuals who in one way or another contributed and extended their valuable time and assistance which let to completion of this thesis. First and foremost, my utmost gratitude to Assoc. Prof. Rostislav Choteborsky, Ph.D., Department of Material Science and Manufacturing Technology through whose sincerity and guidance I was able to complete this thesis. I am thankful to my advisor, Ing. Adam Kesner for helping me in my thesis. I would like to thank Lucie Mareckova for supporting me in academic arena. I would like to count my Czech friend Kristina Adamkova for helping and instructing me in lab and translating Czech to English whenever it was necessary. Thanks go to my all professors who taught me during my whole study period and to my classmates and friends especially Emmanuel Safro for being always supportive to me in different ways directly or indirectly. Thanks go to last but not the least, my family and relatives.

Special thanks go to Head of Department and staffs of Czech University of Life Sciences (CULS), Faculty of Engineering, Department of Material Science and Manufacturing Technology's Laboratory.

Table of Contents

List of Figures

List of Tables

1. INTRODUCTION

1.1 BACKGROUND OF THE STUDY

Iron alloy is one of the vital elements since the medieval time due to its wide range of applications in various fields. It is mainly used in transportation, agriculture, machining and construction, etc. Such wide range of uses is possible due to the excellent properties of Iron alloys.

The major drawback associated with iron alloy is its low wear strength. Wear causes problems on materials and its components such as deterioration of mechanical properties and overall alternation of the machine and building precision. It's not only limited here; it can also be fatal and may lead to economic burden.

Machinery are mainly used to increase the productivity on agricultural farmlands, food and processing and almost all types of industry. Nevertheless, the equipment leads to failure due to high wear rate and often needs to be replaced as it can no longer perform its function.

This study is conducted to overcome the above listed problem of wear in our working environment and to understand the abrasive wear of iron alloy, chemical composition of the material and its significance, microstructure of the material and means to improve the properties of the iron alloy so that it can resist the abrasive wear on the materials mainly used as a machine or operating components in the agricultural sector.

1.2 AIM OF THE STUDY

The aim of this thesis is to determine the abrasive wear of the iron alloy with addition of boron as an alloying element and to compare between two test materials, it is proceeded as follows

- Multiphase of iron alloy.
- High carbon iron alloy.
- Effect of addition of different alloying elements.
- Mathematical model of the multiphase iron alloy.
- Wear mechanisms.
- Wear test of chosen iron alloy with boron content and the prediction of the wear rate.
- Feasibility of the chosen iron alloy.

2 LITERATURE REVIEW

2.1 PURE SYSTEM OF Fe – B

Alloying element like boron, even in small addition, is well known to improve hardenability of steels (Furtado et al, 2011). Among the binary systems consisting of a transition metal (TM) Borides Characterized by their practical importance and fundamental interest for science, Technology and industrial applications (Bialon, 2013). Examples of important properties are high melting Temperatures, high hardness, good creep resistance, high electrical and thermal conductivity (Ivanovskii, 2012). And chemical stability and inertia, which makes the transition metal borides ideal Materials for resistance to oxidation at high temperature (Kaner, 2005).

Recently, the in these materials, was renewed due to the discovery of super-hard ReB_2 (Gilman et al, 2006). Its synthesis follow-up of a new principle of design of new ultra-hard materials by combining small, strong covalent bonding of the elements with large, electron-rich transition metals (Levine et al, 2009).

Iron borides, which are formed in the microstructure of high-boron steels, improve tensile strength (Jimenez et al, 1995). Steels, while hardenability of boride steels decreases when the hardening capacity Refers to the amount of dissolved boron at the grain boundaries (Watanabe et al, 1983). The heat treatment during the production of certain temperatures results in the formation of borides. Whereby the influence on the toughness of the steels is reduced (Watanabe et al, 1983).

There are different opinions on the positions of the boron atoms in the crystal lattice of iron. On the basis of the comparison of the diffusion coefficients of carbon and boron and Jandeska I. J. Morral found that the boron atoms in the γ-Fe lattice are dissolved interstitially (Sudo et all, 2015). C.B. McBride, J.W. Spretnak and R. Speiser obtained the same results on the basis of the comparison of the theoretical examination of boron atom radius with the interatomic distances in γ-Fe lattices. However, these geometric considerations ignore the physical and chemical mechanisms of bonds.

They also found that the difference between the lattice parameters of pure iron and iron containing boron decreases with increase in the temperature and it leads more boron atoms

to drift to the grain boundaries where the separation of boron has been found (Thevenot, 1991).

Abrasive wear resistant can substantially be improved by second phases embedded in a hard or soft matrix (Gahr, 1987). Conventional Fe-base wear-resistant materials take carbide as wear-resistant phase, such as high chromium cast iron and Ni-hard cast iron, which would consume a large amount of expensive alloying elements (Pertek et al, 2003). Boron is an inexpensive material and is widely used in steel production and usually possess very high hardness, which is widely used to increase the wear resistance of surface layer via the boriding process (Li, 2008).

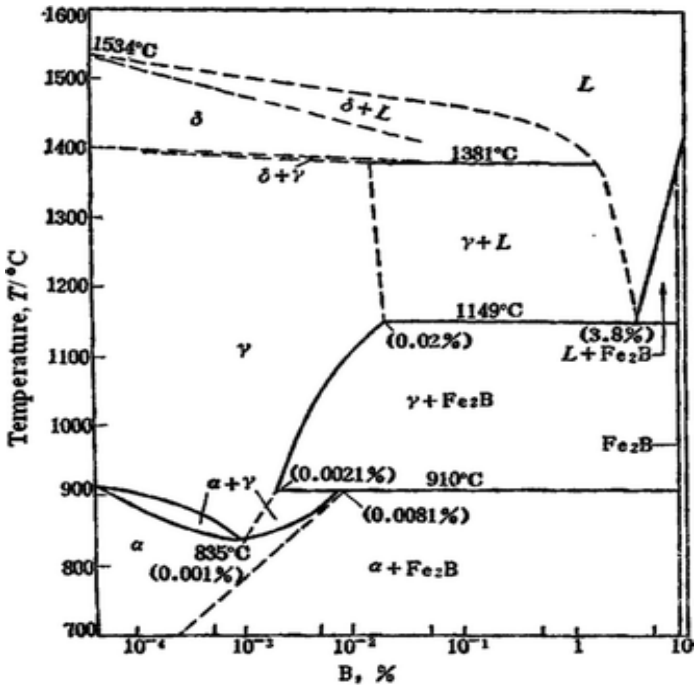

Figure 2.1 Fe-B phase diagram (Yi et all, 2011)

The Fe-B phase diagram *Figure 2.1* above, boron has a very low solubility in iron (maximum iron solubility of 0.02 % by weight and iron 0.0081 % by weight), which constitute the boride formation possible, when boron is added to molten iron. Boron replaces carbon in cast iron structure and eutectic borides supplanting eutectic carbide in microstructure as hard wear safe stage.

The dissolvability of boron in iron is either in austenite 0.02 wt. % at 1,149 °C or in ferrite lower than 0.000 4 wt. % beneath 727 °C contrasted and generally high carbon solvency of 2.11 wt. % at 1,148 °C in austenite and 0.0218 wt. % at 727 °C in ferrite which makes boride

structure when boron expansion is more than its solvency in ferrous compound (Xiang et al, 2010)

This alloy can be prepared by adding more boron into Fe alloy; In fact, the boron Fe_2B formation is preferred with boron content of more than 0.0021 % by weight as seen in the *figure. 1*.Lakeland et all (1992), proposed the idea to use the boride as wear-resistant skeletons and for the first time produced high boron cast alloy.

Xiang et al cited that the lattice comprises of fine pearlite in the amalgams with and without adjustment, however the grain size of the grid is diminished extraordinarily after alteration then in the wake of extinguishing at 1,303 K and hardening at 473 K the framework of the compounds for the most part changes to slat type martensite, for the combinations without change the boride morphology remains practically unaltered after warmth treatment.

Correa et al found that boron decline the dissolvability of carbon in austenite delivering an expansion in the quantity of carbide cores and henceforth a substantial number of fine carbides in the set structure and furthermore expansion of boron expands the wear opposition of white iron by 40 % by and large; such an improvement was credited to the microstructural refinement of carbide stage which is the fundamental wear obstruction in spite of the fact that lattice likewise assume an essential job additionally martensite network diminishes wear and carbide break more to the point the auxiliary carbide fortify the martensite grid which thus builds the mechanical help to the carbide stage (Ma et al, 2010)

Correa et al noticed that the optional precipitation in high boron white cast iron at various hardening temperature with increment of boron content made the dendrite structure gradually disappear while the essential stage gets the type of segregated portion encompassed by eutectic cells. The matrix and the wear-resistant phase could be here controlled by changing carbon and boron concentrations, it approaches created possibility to design the material with the required microstructure. Moreover, high boron Alloy formed consumes a relatively small amount of expensive Alloy elements with good abrasion, high thermal neutron resistance and resistance to corrosion, etc (Ma et all, 2012).

Hypothetically, it is observed that the boron atoms segregate at austenite grain boundaries and then reduce energy with magnitude less the 1 % but with certain shapes of ferrite nucleus under proper conditions, the energy reduction can point to a nucleation rate reduction by a

factor of 10 on grain boundaries of austenite. That is why boundary energy reduction of austenite grain is a major mechanism contributing to hardenability (Morral, 1977).

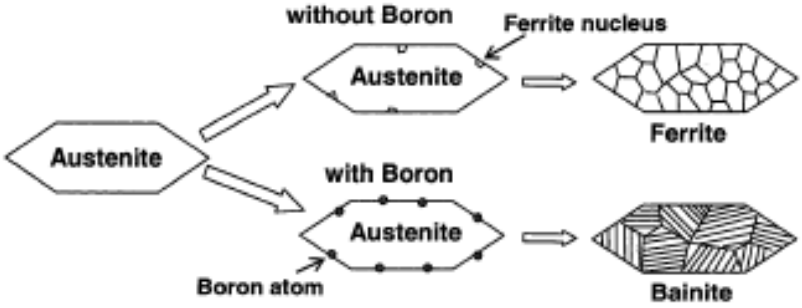

Figure 2.2 Reduction in the number of nucleation sites for ferrite with boron addition (Lu,2007)

In the above *Figure 2.2* (Lu, 2007), the segregation of boron to the austenite grain boundaries can reduce the diffusivity of iron, and possibly the jump frequency of carbon, by blocking interstitial sites or by increasing the grain boundary modulus also a reduction of carbon jump frequency at austenite grain boundaries can result in a retardation of ferrite nucleation on these boundaries (Lu, 2007).

It is possible that boron atoms can diffuse on some regions with low atomic density which is preferred for the nucleation of ferrite and position themselves through precipitating some very small-sized particles, the nucleation rate of ferrite will be reduced (Guttmann et al, 1979).

2.2 SYSTEM OF Fe – B – C

Alloys based on iron with increased boron content have high wear resistance and they satisfy requirements occurring about the intensification of technological processes. However, use of these alloys is limited by their high brittleness making it difficult to manufacture one-piece and bimetallic articles and reducing their durability under different operating conditions (Shen at el, 1990). The consequence of boron on hardenability also depends on the amount of carbon in the steel. The essence of boron increases in inverse ratio to the part of carbon present (Yi et al, 2011).

Features of solid solutions formed in alloys of the system Fe-B-C relate to the presence of two interstitial elements: boron and carbon. Formation of interstitial phases of the composite type should be accompanied by loosening up of compact lattices leading to a change in

boundary for the region of homogeneity, and the occurrence of areas with local enrichment of components causing structural in homogeneity of solid solutions (Spiridonova, 1984).

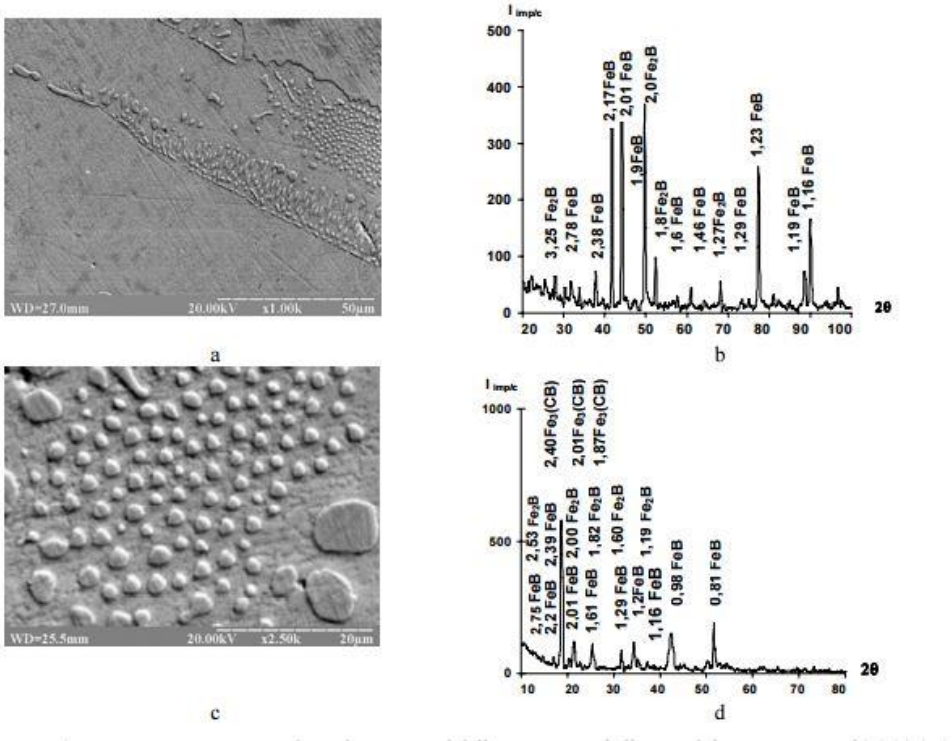

Figure 2.3 Microstructure in secondary electrons and diffractograms of alloys with boron content of 9.0 wt. % and carbon content of 0.2 % (wt.) (a, b), with boron content of 11.0 wt. % and carbon content of 0.4 % (w.t) (c, d). (Ya et al 1988)

On the basis of results from the above *Figure 2.3* Filonenko (2013) obtained values of microhardness for boride phases with values of microhardness for these phases for binary Fe-B alloy, which is not alloyed with carbon and conclude that in the process of carbon alloying the microhardness of iron monoboride and boride is considerably decreased. According to its results for alloy with boron content of 11.0 wt. % it pointed that if temperature of monoboride FeB formation is 1,843 K (31-34), then in the process of alloying with carbon this temperature decreases and under carbon content of 0,1 % (w.) to 1,733 K, and for carbon content of 0.4 % (w.) equals to 1,712 K. In the thermogram of the alloy having a boron content of 11.0 % (by weight). And a carbon content of 0.4 % (by weight). At a temperature of 1,596 K, a thermal effect probably corresponds to the eutectic transformation $L \rightarrow + Fe_2B + FeB$. The final thermal effect in the thermogram at a temperature of 1,425 K

corresponds to the transformation in the solid state. This transformation refers to the polymorphic β - Fe (B, C) → α - Fe (B, C) transformation of the elevated temperature modification β - Fe (B, C) to lower temperature modification (Zatuska, 1983).

It can be assumed that the transformations in the temperature range of 1,420-1,480 K occurs as the result of carbon effect. Because carbon solubility in FeB and Fe_2B borides is low, presence of carbon in iron borides is determined by availability of odd vacancies (Samsonov et al, 1999), which along with carbon atoms set up the stable complexes. Iron monoboride FeB has homogeneity region, and at high temperatures carbon solubility is higher than one at low temperatures. Probably, within the temperature interval of 1,420-1,480 K depending on carbon content decomposition of supersaturated with carbon monoboride FeB takes place, at which point boron cementite $Fe_3(CB)$ is forming (Baklanov et all, 2015).

The matrix of wear-resistant iron--boron--carbon alloys is formed because of successive multiphase crystallization: eutectic and peritectic. Based on iron boride Fe_2B there is growth of eutectic colonies of Fe-Fe_2B inheriting features of the sectorial structure of the basic crystal. A bi-crystal has a prismatic morphology described in detail in the monograph (Yu, 1978).

Paju et al (1991) saw that boron can enormously expand the hardenability of steel with a little sum, yet its impact is diminished rapidly with the expansion of carbon content. The framework comprises of perlite and martensite however with little level of pearlite, the lattice changes to martensite after warmth treatment yet the boride morphology is constantly unaltered.

High boron white give iron takes boride a role as reinforce stage and take care of the issue of low sturdiness of network and replaces carbide in high chromium white cast iron in the meantime diminishing the carbon content in high chromium white cast iron to a dimension for fortify and intense framework since boride have higher hardness than carbide (Ya et al 1988).

2.3 SYSTEM OF Fe – B – C – METALS

Mechanical properties of high boron steel with various aluminium and chromium concentrations in Fe-B-C-Cr-Al have been were investigated by (Zheng, 2016) where the results indicate that aluminium and chromium elements are when added synchronously, the as-cast microstructure changes to α-(Fe, Al, Cr) solid solution, $(Fe, Cr)_2B$ boride, $M_7(C, B)_3$ and $M_{23}(C,B)_6$ borocarbides.Moreover, the nucleation and growth of $M_7(C, B)_3$ borocarbide is adhere to $(Fe, Cr)_2B$ boride because of an interphase match between crystal plane (101(-) 0) of $M_7(C, B)_3$ and (010) of Cr-rich $(Fe, Cr)_2B$. Alloy Fe-1.46 wt. % B-0.22 wt. % C-11.92wt. % Cr-8.73 wt. % Al shows the highest impact toughness value. The main fracture mode is brittle fracture of boride and tough fracture of matrix (Lv et all, 2016).

The mechanical modulus and hardness of borides hard phase were investigated by (xing,2016). The results from the experiment show that the type of hard phases in Fe-Cr-B-C alloys is Fe_2B and Fe_3B, and their morphology is the continuous network. The mechanical modulus and hardness of Fe_2B are higher than Fe_3B and the addition of chromium in the Fe-B-C system can improve the mechanical modulus and hardness of Fe_2B and Fe_3B (Rottger et all, 2015).

The presence of the amorphous matrix with a high hardness and plasticity and inclusions of boride phases of titanium in the case of Fe67Ti7B2C2 alloy provides lower linear wear and a reduction in its rate during the experiment conducted (Borisov at all, 1987). Moreover, the paper stated that the presence of a large quantity of hard and brittle FeB and Fe_2B phases with a low amorphous phase content in the Fe61B37C2 alloy coatings somewhat reduces their wear resistance.

Addition of elements such as Ni, which do not form carbides (or when they are not able to form cementite), does not change the microstructure of the alloy steel formed after the transformation. Only a small portion of these elements can be added to the steel from graphite moulds during processing, with the decline in steel properties. (Foll, 2016)

Table 2.1 Rockwell hardness and microhardness by (Zheng Lv, 2015)

Samples	Rockwell hardness (HRC)	Microhardness of the matrix (HV)	Microhardness of M_2B (HV)
Co	30.5	236.8	1186.8

C_1	45.9	414.5	1172.5
C_2	51.9	423.8	1523.2
C_3	57.4	434.8	1658.6
C_4	57.6	446.4	1716.1

As per *Table 2.*1, Rockwell hardness and microhardness were found with increase in aluminium and chromium concentration. The microhardness of borides was found to be higher with higher chromium content. The research concluded that the addition of chromium is beneficial to the impact toughness of the high boron steel. The highest impact toughness for the alloy Fe-1. 46 wt. % B-0. 22 wt. % C-11. 92 wt. % Cr-8.73 wt. was found to be 5.67 J.cm^2 as shown in the *Figure 2.4* (Zheng Lv, 2015).

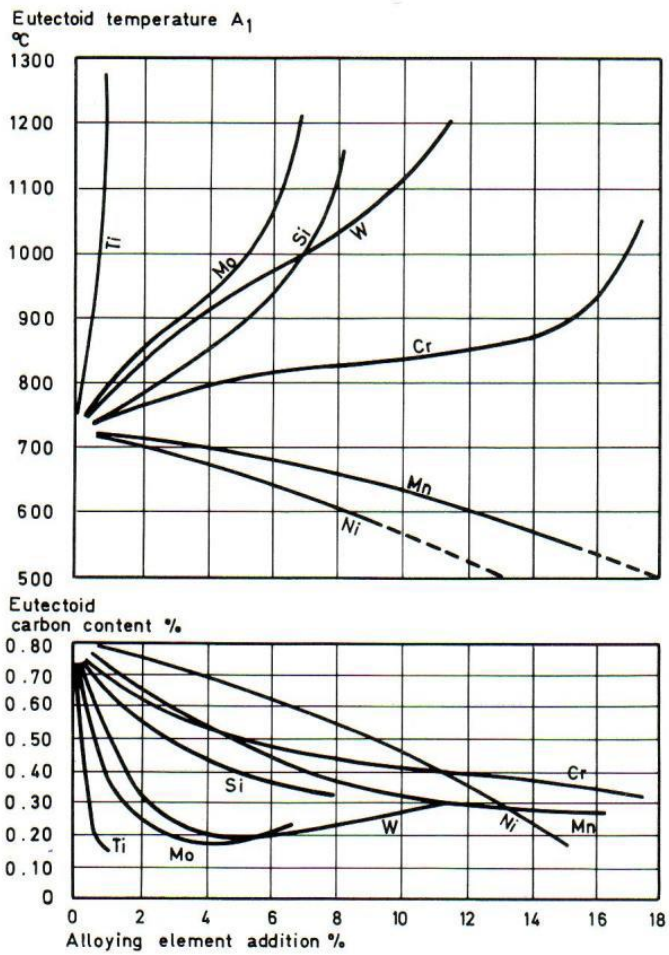

Figure 2.4 Influence of alloying element additions on the eutectoid temperature and the eutectoid carbon content (M. Maalekian, 2007)

2.4 INFULENCE OF Cr ON EUTECTOID POINT AND MECHANICAL PROPERTIES OF BORIDES

Chung et al. (2013) added that boron expansion in high chromium smelt was the main reason for access to M_7C_3 carbide as an essential step and increasing its volume as it was the major step of strong nucleation, thus decreasing the resistance thus obtained. The force increases the hardness and wear of the material. Liu et al. (2008) found that the precipitation of dendrites by additional precipitation in boron-rich boron at different curing temperatures and increasing boron content gradually disappeared, while the essential state was the island type. closed to eutectic cells.

High boron iron gives Borid a reinforcing role, solves the problem of low grid durability and replaces carbide in high chromium cast iron, reducing the carbon content of high chromium cast iron at a level that can be improved and an intense network, the boride has a higher hardness than carbide (Ya et al., 1988)

Changqing et al. (2003) confirmed that the extension of the solubility of boron in Fe-Cr-B melt gave the impression that it was associated with other metal constituents with a larger core width than that of iron. that this structure represented an endless substitution force. Arrangement with iron, for example, Cr, Mo and V In addition, the cast and treated melt and fused martensite F-Cr-B is highly immersed in boron and carbon in boron and carbon, with a solubility of boron most probably between 0.185 and 0.515 percent by weight. as cast and 0.015 to 0.058% by weight. % in the processed state.

Expansion of the chromium and carbon content in the tinplate modifies the eutectic carbide from constant M_3C to moderately irregular M_7C_3, resulting in increased strength. More than 12% In% Cr, the eutectic carbide passes to the M_7C_3 type, which is regularly represented in intermittent or lamellar form. The M_7C_3 thread has a higher hardness of about 1,400 to 1,600 HV, as opposed to the persistent M_3C carbide with a hardness of about 1,000 HV in chromium-plated iron with a lower chromium content. Among the traditional destabilizing, E7C3 eutectic carbide is contained at 10-25% by weight. In any case, the % Cr iron does not seem to undergo any further modification in the 30% by weight. From Cr iron, an advance of M_7C_3 to $M_{23}C_6$ was observed in the eutectic carbides of this result in a eutectic duplex carbide structure consisting of the M_7C_3 center, which is surrounded by $M_{23}C_6$ shells, this

modification being within the limits of the content. The extremely high chromium of the light observes the fact that the $M_{23}C_6$ carbide is stable, especially with high chromium content (Higgins, RA 1993).

2.5 MULTIPHASES OF IRON ALLOYS

Steel and cast iron are portrayed to a great extent by iron carbon phase diagram shown in the *Figure 2.5* below. Unadulterated iron has three types of allotropies which are strong iron and magnet stage progress at 770 °C and expansion of carbon present heterogeneous stages which incorporate eutectic point at 4.3 wt. % C at 727 °C which comprise of three strong stages being austenite-carbon strong arrangement, ferrite-carbon strong arrangement and cementite. Iron is polymorphous component which exists in two precious stone cross section structure that is body cubic focus (BCC) alpha and delta and face cubic focus (FCC) gamma iron. The material changes happen in unadulterated iron which results in arrangement of three diverse single stages in iron-rich composites which are as per the following: (ASM Handbook, Vol 2, 1990).

A - interstitial strong arrangement of carbon in alpha iron body cubic center (BCC)
Austenite – interstitial strong arrangement of carbon in gamma iron face cubic focus (FCC) and δ - iron body cubic center (BCC).
Schematic diagram of iron carbon phase diagram (ASM Handbook, Vol 2, 1990).

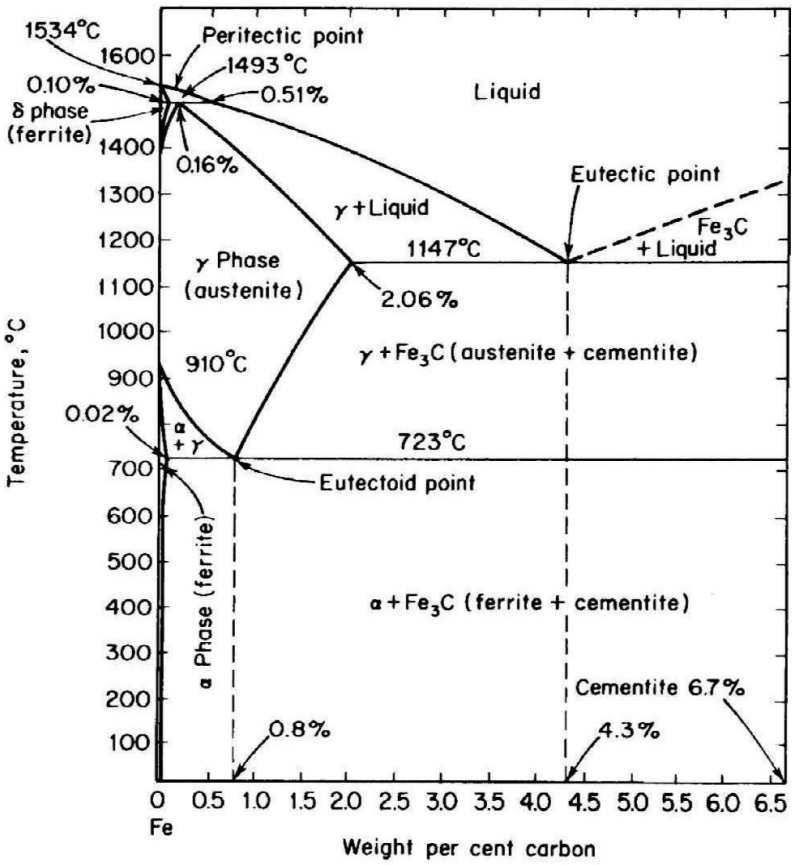

Figure 2.5 Schematic of iron carbon phase diagram (ASM Handbook, Vol 2, 1990)

Austenite - interstitial strong arrangement of carbon in FCC iron shaped by cementing from fluid, vast grains and straight grain limits, stable at raised temperature, high solvency for carbon, high pliability and formability. Ferrite interstitial strong arrangement of carbon in BCC iron shaped from austenite through strong stage change, little grains and unpredictable grain limits, stable at room temperature moderate dissolvability for carbon, pliable and delicate not all that solid. Pearlite composite structure of laminar ferrite and cementite, framed as an item eutectoid change from austenite, great consolidated rely upon the morphology (strip cementite), (ASM Handbook, Vol 2, 1990).

Hypoeutectic steels of not exactly wt. 0.77 wt. % C, these records for low and medium carbon steels, microstructure comprise of pearlite and proeutectoid ferrite. The extent of pearlite increments with expanding wt. % C towards 0.77 wt. % C. Higher segment of pearlite makes the steel more grounded yet less bendable. Hypereutectoid steel of more prominent than 0.77 wt. % C, these records for high carbon steels. Microstructure comprises of pearlite grid and cementite organize along grain limits, cementite arrange lessens sturdiness and malleability altogether, extent of cementite increments with expanding with carbon content far from 0.77 wt. % C. At whatever point fluid carbon is 0.55 wt. % C responds with delta ferrite bcc ɗ̂ 0.8 wt. % C it changes over it to gamma austenite strong arrangement FCC ɣ 0.18 wt. % C at the temperature of 1,495 °C bringing about peritectic response. Fixed fluid carbon 4.3 wt. % C) separates into gamma austenite strong arrangement FCC ɣ 2.06 wt. % C and iron (cementite) carbide Fe3C 6.67 wt. % C at a temperature of 1,148 °C which shapes eutectic response (ledeburite). Also, gamma austenite strong arrangement FCC ɣ 0.8 wt. % C separate into alpha ferrite strong arrangement BCC α 0.025 wt. % C and iron cementite carbide Fe3C 6.67 wt. % C at the temperature of 727 °C which frames eutectoid response (perlite). Besides, the stage change can persistently change to satisfy the need of that work dependent on both Continues Cooling Temperature (CCT) process and the Time Temperature Transformation (TTT) outline underneath (ASM Hand Book,Vol 2, 1990).

2.5.1 TIME TEMPERATURE TRANSFORMATION

TTT outlines are less of significance since a compound must be cooled rapidly and afterward kept at a temperature to take into consideration particular change to happen. Be that as it may, most mechanical warmth medicines include constant cooling of an example at room temperature. Subsequently, CCT outlines are commonly increasingly proper for iron carbide stage in designing applications as parts are cooled through a required medium from a handling temperature which is more monetary than exchanging to a different heater for an isothermal treatment. CCT charts demonstrates the degree of change as a component of time for a constantly diminishing temperature. For persistent cooling, the time required for a response to start and end is postponed, in this manner the isothermal bends are moved to longer time and lower temperatures. These charts permit forecast of the microstructure after some time for steady temperature and persistent cooling heat medications individually (William D Callister 2004).

2.5.2 CONTINOUS COOLING TRANSFORMATION (CCT)

CCT stage chart diagram as shown in the *Figure 2.6* is generally utilized when heat treating steel. These outlines are utilized to speak to which kinds of stage changes will happen in materials it is cooled at various rates. These graphs are regularly more valuable than TTT outlines since it is increasingly advantageous to cool materials at a specific rate than to cool rapidly and hold at certain temperature. Quick cooling of hardenable steel at 65 °C for 56 seconds' outcomes in martensite while for medium cooling at 154 °C for 792 seconds' progressions to banite then at last moderate cooling at 538 °C for 18,803 seconds' progressions from banite to ferrite + pearlite. The two charts are one might say, stage with included parameter in type of time likewise part of begin and completion of each bend relies upon grain size of austenite, concoction organization and temperature of austenite. (William D Callister 2004).

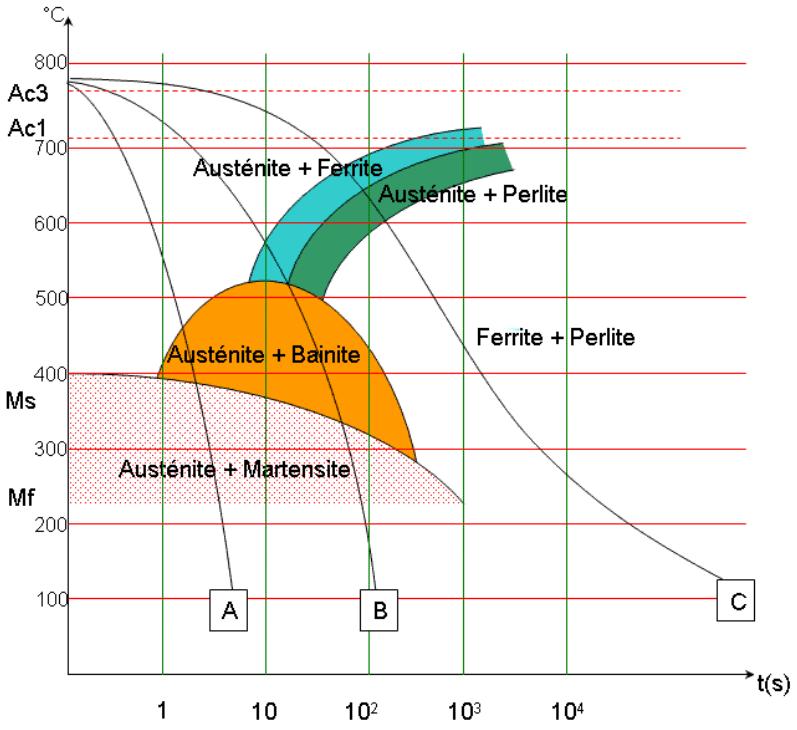

Figure 2.6 Continuous cooling transformation diagram. (William D Callister 2004)

3 WEAR OF COMPOSITES

Composites Composite matrices (MMC) are highly weight-saving, well-protected against scratches and protected against shaking, with high dimensional stability and optimized operating temperature. MMCs are made by dispersing a fortifying material in a metal grid. Carbon yarns are typically used in aluminum mesh to orchestrate composites with low thickness and high quality. The network is a solid material in which the fortification is implanted and is totally non-stop. Fortification is generally not a simple basic commitment but is also used to modify physical properties such as wear resistance, network coefficient, or hot conductivity.

Sintered MMCs are made from a high-alloy steel grid containing coarse, coarse, hard particles with low iron reactivity, such as titanium carbide (TIC). Composite metal structure dependent on the curable steel grate (extinguished) with incorporated hard particles, has a toughness far superior to that of molded materials under special conditions and low sintering action of these round powders. The reinforced metal mesh composite particles dependent on the viruses working steel are increasingly used as wear resistant material because of its better wear properties than normally used, which justifies their application, especially in the mining and mining industries where white cast iron is generally used against the wear and tear of minerals, (Sebastian et al 2007).

Zum gahr (1987) noted that in the case where the container demands to make the materials impervious to stains, it is important to homogeneously circulate a certain hard particle substance in the metal frame. The inserted particles, for example tungsten carbides, influence the reliability of the microstructure, increase the hardness and improve the wear resistance of the metal amalgam. Chatterjee et al (2006) proposed that the idea of difficult steps and the type of grid harmonize the harmony between the metal structure and the difficult steps that reinforce the wear attributes of the materials in the workplace.

Sapate (2004) states that substance, singular hardness, hard particle size and roughness depend on rough wear, and that their viability depends on the connection between the wear instrument and the microstructure of the wearer. multiphase material. Polka et al. (2009) explained that the task of dispersing the separated particles between carbides was to study a

more conclusive division of carbide size and volume in dry sand elastic wheel wear tests in accordance with the standard ASTM G65.

Badisch et al (2003) predicted that obstruction of materials by wear is structural or by metallurgical precipitation of essential hard steps, or by fortification of artificially mixed carbide raw materials, and also claimed in (2009) that the appropriation of particles in the composite of the metallic network and other microstructural parameters The size of the molecules and the volume division are key factors to preserve the vital effect of the abrasives which attenuate the carbide cracks and increase the opposition wear (CIAT). In addition, the hardness of the hard-confronting framework does not only depend on the creation of the essential segment substance used in the network plane but also the carbide weakening among the high temperature manipulation innovation.

Kumar et al. (2010) predicted that the microstructure of the composite examined in practice would be highly constrained by parameters such as media thickness, network amalgam, shape temperature, shape velocity and metal mixing. liquid before casting the enrichment particles add to the area with more volume division enrichment particles enhance the properties of the network of compounds both mechanically and tribologically, allowing them to be used in modern applications and automotive applications. MMCs are exceptionally useful in companies such as automotive, aviation and development, where these exercises are normal.

3.1 ABRASIVE WEAR

This type of wear occurs between two metal segments that slide against each other under a connected load in a field where no abrasives are available. The name is accomplished because of the difficult material connection between the severities outside the materials in contact. Grid wear is the unity of the material between two surfaces in relative motion, caused by the sliding of hard particles between the surfaces in contradiction; the hard particles glide smoothly over a softer surface and separate the materials from those last mentioned, under the ordinary load, the severities of the hardest surface embedded in the softer surface producing disfigurement of the plastic (Harris et al, 2002).

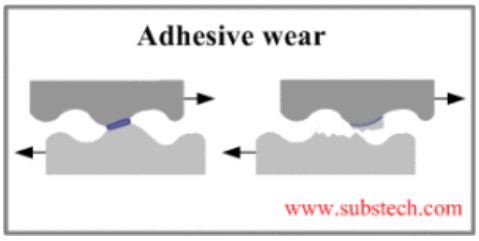

Figure 3.1 Schematic view of Adhesive wear (Harris et al, 2002).

Two body abrasion shown in *Figure 3.1* and three body abrasion shown in *Figure 3.2* differ from each other and has distinctive characteristics. In case of two-body network wear, the friction surface moves openly, and the wear is caused by a hard projection on one or two surfaces. In three-body wear, the scraping molecule is allowed to roll and slide between two surfaces as interfacial components and, in any case, any material concerns, for example, high pressure, low pressure and gouging. High pressure is caused by solidification of the work. The low pressure is due to the slight scouring action of the grating particles that scrapes the metal surface without solidification work. Gouging results in high pressure forming grooves on the affected material (Avery H.S., 1977).

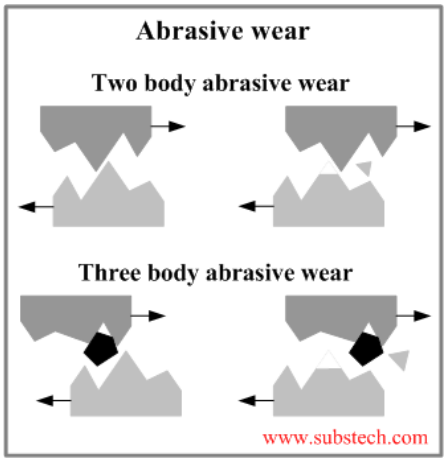

Figure 3.2 Schematic view of two bodies and three bodies abrasive wear (Avery H.S, 1977).

3.2 WEAR MECHANISM

Traces of wear and plastic torsion decrease as the group of boron composites increases. In addition, it is found that the wear trace of the dipped examples is deeper than that of the molded examples due to the low hardness it should be. In light of Mustafa et al (2015), we

are particularly trying to measure the high carbide content in the examples with a high boron content in order to improve the wear resistance of the material. in addition, the use of thermal drugs to obtain a martensitic network reinforces the obstruction due to wear under a scraped point at low pressure and finally, in sliding conditions, the martensitic grid reduces the wear frame and thus decreases the breakage of the carbide. The instrument of wear among the use of the network is affected by some factors, for example, the molecule, the material and the relative state, delicate and hard.

3.3 RELATIVE SOFT PARTICLES

Most of the time, rough wear should occur on a delicate metal surface scraped by a hard, sharp molecule. The materials used are lighter than the characteristic rough soils, so that devices causing serious scratches cause serious scratches, causing the newly sharpened edges to weaken Natsis et al (1999). According to Natsis et al. (2008), the wear rate of the culture instruments depends on the dirt particles.

Scheffler et al. (1988) argued that the exterior of the scraped steel sand was generally smooth and uniform with respect to the muddy soil. This is explained by the fact that the muddy soil contains rough particles firmly held. They found that steel scars on stony ground were deep and dug holes where material had to be pulled from the surface. The hardness of the materials used for assembly is also a central point in the assurance of soil wear. The creation of the mixture and the hardness of the material used are some of the components that influence the rate of wear of the plough.

Another factor affecting wear is the moisture content of the soil; per Miller (1984), the impact of moisture on the wear rate of growing equipment depends on the type of soil and differs from sandy soils compared to muddy soils. Ferguson et al (1998) and the sawmill operator (1984) found that soil, moisture, substance and total soil influence were influenced by the grower in some locations in Australia.

3.4 RELATIVE HARD PARTICLES

Moore (1974) pointed out that the surface undergoes strong solidification, that is, wear is related to the quality of the material and the hardness of its surface. It must be identified with the hardness of the mass in a thin assembly of materials where the rate of deformation

Solidification appeared as a component of the hardness of the mass, as in the heat treatment of the raw carbon steel.

The wear rate of all shares is higher in soils with increasing sand fraction; the main factors affecting wear rate include chemical composition, hardness being the most dominant (Bobobee et at 2007) The wear characteristics of a soil are related to the type of abrasive and stones present (Zhang and Kushwaha 1994).

Richardson (1968) represented his result by the various methods of decomposition of distinctive coarseness sizes. Moore cited Richardson who determined that the 19 to 38 mm wide cut stones were responsible for more than 50% of the total wear volume, despite the fact that their volume range in dust was less than 1.4 %. Johnson (1960) stated that network collection was increasing rapidly as the size estimate diminished.

3.5 MATERIAL (PARTICLE)

Zum Gahr (1998) deduced in his investigation that the progress of the loss of wear of the material depended on the properties of the coarse particles and the wear material, just as the working condition depended on the proportion of the hardness of the scraped particles. relative to the hardness of the material and the expansion of the lower to upper wear dimension of the multiphase material begins and ends when the network hardness and hardness of the reinforcement phase are individually exceeded by the hardness of the network particles and furthermore by the size of the grating, the normal load and the speed of effect finally, the edge effect without thinking of the lubricant carriers as they appear in the figure.

Moore et al (1983) showed from the *Figure 3.3* that hypothetical expectations and test results asserted that the shape of the molecule had an impact on wear. If the charge of the molecule and the hardness of the surface are consistent, the intended plastic contact zone will be stable, but the transverse territory of a groove resulting from such contact will depend on the shape of the molecule. Deuis et al (1998) concluded that the hardness of the grating particles could affect the wear rate.

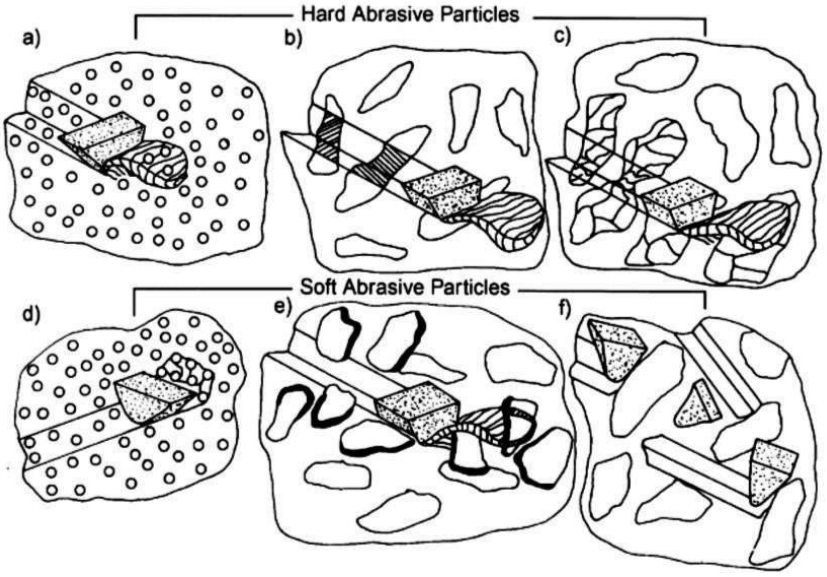

Figure 3.3 Reinforcing phases along with sliding hard or soft abrasive particles (Moore et al, 1983).

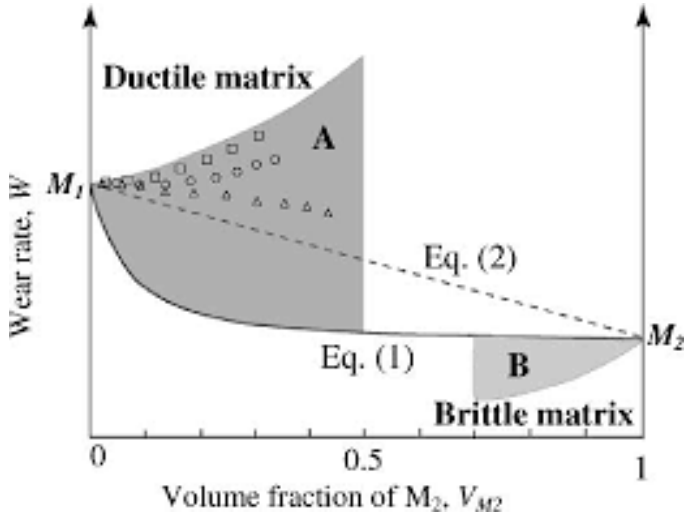

Figure 3.4 Predicted abrasive wear rates of composites. (Anex and Jacobson, 1994)

In above *Figure 3.4*, the abrasive wear rate of the composite decreases linearly with increasing volume fraction of reinforcement.

$$\frac{1}{W_c} = \frac{V_{M1}}{W_{M1}} + \frac{V_{M2}}{W_{M2}} \qquad \text{(Eq.1)}$$

which was introduced for two-phase composites by Khrushchev and Babichev (1953) assumes that the components of the composite wear at an equal rate and the second wear equation

$$W_c = V_{M1} W_{M1} + V_{M2} W_{M2} \quad \text{(Eq.2)}$$

for multiphase materials, introduced by Zum-Gahr to explain experimental data, is the linear rule of mixtures, here, the wear behavior of a composite is not dominated by a single phase. where W and V are, respectively, the wear rates and volume fractions of the matrix (designated by subscript m) and reinforcement (designated by R). Note that the wear resistance, R, in Khruschov's original formulation is given by the reciprocal of the wear rate, R = 1/W.

This expression was also derived by Axen and Jacobson (1994) using the equal pressure assumption that all components of a composite carry the same specific load. A cyclic wear model for oriented fibre composites that predicted narrower bounds for abrasive wear behaviour was proposed by Yen and Dharan (1996). In their paper, fibre instability due to preferential wear of the softer matrix resulted in cyclic generation of wear debris during the wear process. However, interface toughness and other physically based factors were not considered in their model.

3.6 WEAR OF SINTERED METAL MATRIX

The increasing contact due to the connected load allows the raw product to enter the surface, this infiltration of silica sand network particles produces wider and deeper grooves superficially providing cutting and wake activity. superficial because of the proximity of less fortifying molecules to the surface. so that in a strongly enhanced region, the input of the crude molecule is significantly reduced, which contrasts sharply with the less enhanced zone, since the highly enriched district generally has a higher hardness than the composite. In addition, the more prominent holding of the fortification particles with the network combination at the surface carries a load which influences the frame, resulting in less sill activity and less wear of the composite (Mazahery and Shabani, 2012).

3.7 ENVIRONMENT

Stachowiak et al (2005) found that the proportion of raw hardness to hardness of the metal increased with increasing temperature, which resulted in a higher wear rate. Likewise, the

rough three-body wear, the contact between a grid and the uneven surface would be particularly contrasting and this would not happen in the two-body brutal wear mode, so in a three-body scraped area created in the material of disfigurement. spread in the network particles. This causes a warm loosening of the surface material while the network remains intact with its hardness.

Jiang et al. (2004) explained that grating may simply be weakened by moisture to create many new front lines or that the severe size may occur, resulting in the decomposition of cornmeal into fine, non-rough particles, materials rough could be weakened by moisture. Garcia et al (2003) estimated that the increase in temperature caused by plastic distortion within a scraped area was related to slip speed while Harris et al (2002) continued to claim that this could lead to disfigurement of the plastic material, recrystallization and properties of the surface material and approximate wear rate. Roughly, with the expanding temperature, there is a corresponding decrease in the hardness of the well-used material and the expanding, rough material that impacts the temperature, for example, the metals decrease more harshly than the non-metallic gate material

Stochowiak (2000, 2001) added that the loss of wear of the materials is based on the properties of network particles and wear materials, as well as the working conditions and the increasing hardness of the raw molecule. wear can increase by about one to two. demands of magnitude of the dimension low to the height as for the state of the coarse particles

Inman et al (2003) have finally estimated that the increase in temperature also had the effect of causing a type of wear based on the consolidated activity of oxidation and evacuation of the oxide layers by scraped area. The oxidation of steels in the air is considerably faster at 600 ° C than at 20 ° C and as the temperature increases the expulsion of the steel, the oxide becomes progressively enormous.

3.8 SOIL

Soils are an unconsolidated natural problem outside the Earth that has been attempted to indicate the impacts of the hereditary ecological components of the atmosphere, the large scale and the state of microorganisms by attenuating the monitoring of parental materials over a period. Soil has many basic capabilities in virtually all biological communities. The

soil fulfils the support functions for the development of a wide range of plants. It constitutes a design support for the development of establishments, platforms, dams and structures. The contrasts of soil begin with one piece of the world then on another, even with a piece of the patio then on another.

Soil composition is described by the atmosphere, life form, attenuation, base material, and the time required to prepare different kinds of soil. The particles that structure the soil are classified into three groupings by size (sand, sediment and soil). The sand particles are the largest and the mud particles are the smallest here and most soils are a mixture of the three. The overall rates of sand, residue and soil are what gives the soil surface. Soil structure is the game plan of soil particles in small clusters called totals. Soil particles bind to form a global structure, depending on the organization and conditions that determine the form (www.soils.org).

4 HEAT TREATMENT OF Fe – B. – C ALLOYS

Heat treatment may be defined as an operation, or series of operations, involving the heating and cooling of metal or an alloy in the solid state to develop the required properties. There are in general five different forms of heat treatment used with alloy steels. These treatments modify the steel's mechanical properties to suit the end use. These commonly used heat-treating cycles are: Quenching and tempering usually consists of three successive operations:

• Heating the boron steel above the critical range, so that it approaches a uniform solid solution.

• Hardening the boron steel by quenching it in oil, water, brine or salt.

• Tempering the steel by reheating it to a point below the critical range, to affect the proper combination of strength and ductility.

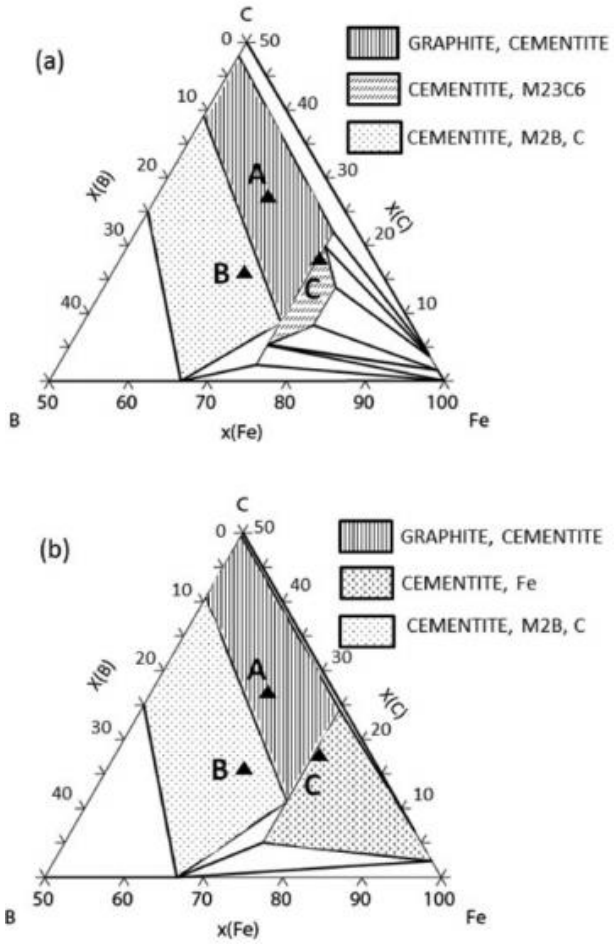

Figure 4.1 The Fe–B–C ternary phase diagram evaluated by the conventional Fe-based alloy database at (a) 1073 K and (b) 1273 K, together with the composition of the Fe–B–C alloys. (Sudo et al, 2015)

Normalizing is a form of treatment in which the steel is heated to a predetermined temperature above the critical range, after which it is cooled to below the range in still air. The purpose of normalizing is to promote uniformity of structure and to alter mechanical properties.

Annealing consists of heating the steel to a point above or within the critical range, then cooling at a predetermined slow rate. Annealing is used to soften the steel, to improve machinability, to reduce stresses, to improve or restore ductility and to modify other properties.

Spheroidize-Annealing is a form of heat treating which requires prolonged heating of steel at an appropriate temperature, followed by slow cooling to produce a globular condition of the carbide. This treatment produces a structure which may be desirable for machining, cold-forming or cold-drawing, or for the effect it will have on subsequent heat treatment.

Stress Relieving is the process of reducing internal stresses by heating the steel to a temperature below the critical range and holding this temperature for a time interval sufficient to equalize the temperature throughout the piece. The object of this treatment is to restore the elastic properties of the steel or to reduce stresses that may have been induced by machining, cold-working or welding. (Khurmi and Gupta,1981)

In the *Figure 4.1* above boron steel outstanding feature is the improved hardenability even by addition of minute quantity of boron. It is generally accepted that peak hardenability occurs when the amount of boron is between 3 and 15 ppm. If excessive amount of boron (> 30 ppm) is present, the boron components are separated in the grain boundaries of austenite, which not only reduces the resistance to hardening, but can also reduce the toughness, resulting in brittleness and produce warm cracking. The effect of boron on the healing also depends on the amount of carbon in the steel. The effect of boron increases in proportion to the percentage of carbon present (Herring, 2007).

The boron must be atomic state for to improve the hardenability of which, it is necessary to be effective during the production of steel are taken for boron. Boron may be inefficient if it's state is altered by poor heat treatment. For example, high austenitisation temperature should be avoided because in some boron precipitates occur. The hardenability is highly dependent on the behavior of oxygen, carbon and nitrogen in the steel. The boron oxide boron reacts with oxygen to form (B_2O_3); and with carbon to form borocementite ($Fe_3(CB)$)

and iron borocarbide $Fe_{23}(CB)_6$)); and with nitrogen to form boron nitride (BN). Strong nitride formers like (titanium, aluminum, zirconium) protect the boron from its reaction with nitrogen. The boron steel contains about 5 to 20 ppm of boron if nitrogen is fixed by using titanium in the temperature range up to 1,830°F (1,000°C). The toughness of the is closing linked to austenitisation and is generally said to decrease by heating above 1,830 °F (1,000 °C). Boron steel must be tempered at a lower temperature than the other alloyed steel element of the same hardening ability (Banerji, 1980).

Heat treatment cycles is carried out in a furnace. The boron steels are heated at austenitising temperatures closer to Ac3 temperature ~ 920 °C for certain time, then it is placed in another furnace for 2 hours ~ 400 °C for soaking. After proper soaking, boron steels are subjected to water quenching (WQ), oil quenching (OQ) and air cooling (AC) as per the requirement.

4.1 BAINITIC STRUCTURE

Alloying elements have considerable influence on the kinetics and mechanism of all three types of transformation of austenite to pearlite, bainite and martensite.

Alloying elements that dissolve only in ferrite and cementite without the formation of special carbides exert just a quantitative effect on the transformation processes as seen in the *Figure 4.2* below. Cobalt speeds up a transformation but most elements, including NI, Si, Cu, Al, etc., slow it down.

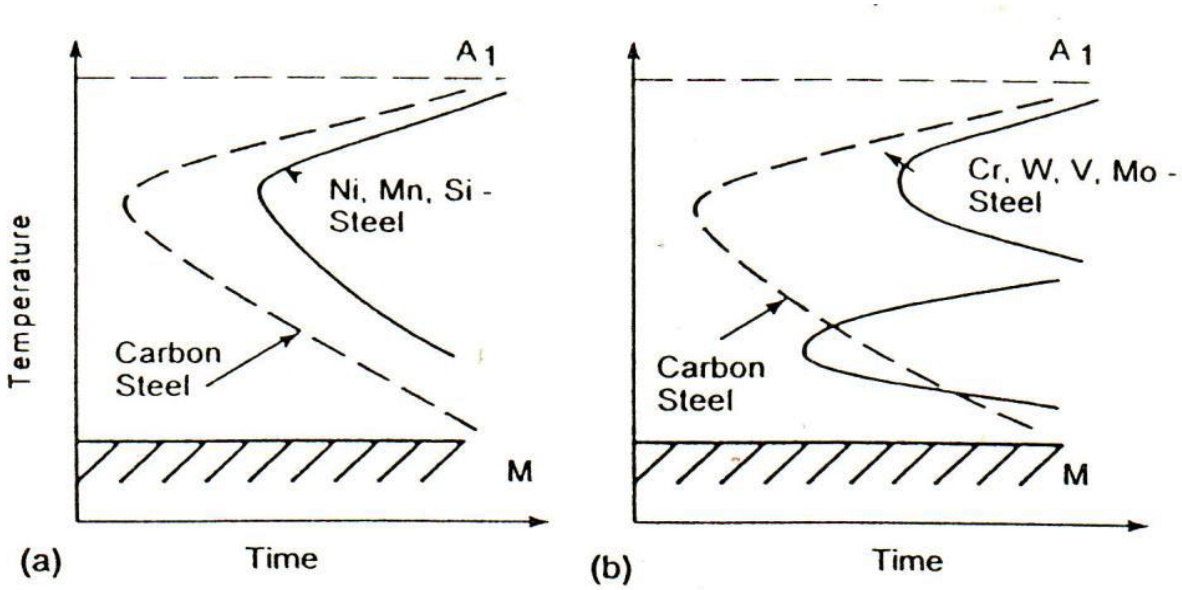

Figure 4.2 Diagrams of isothermal transformation. (a) Carbon steel and steel alloyed with non-carbide-forming elements; (b) carbon steel and steel alloyed with carbide-forming elements. (Khurmi and Gupta,1981)

Carbide- forming elements produce both quantitative and qualitative changes in the kinetics of isothermal transformations in above figure. They (e.g., Cr, Mo, W, V, etc.) influence the austenite decomposition differently at different temperatures:

i. At 700-500 °C (pearlite formation), they slow the transformation

ii. At 500-400 °C, they dramatically slow the transformation

iii. At 400-300 °C (bainite formation), they speed up the transformation.

4.2 BORON EFFECT

Boron is added to steel for only one reason-to increase hardenability. Boron-treated steels have certain peculiar characteristics. (Totten,1997)

1. Boron increases hardenability in hypoeutectoid steel, has no effect on eutectoid steel, and decreases hardenability in hypereutectoid steel.
2. As the austenite grain site becomes finer, the hardenability effect of Boron increases.
3. Austenitizing at high temperature reduces the hardenability effect of Boron.
4. For the maximum Boron effect, the concentration should be in the range 0.0005 to 0.003 wt%.
5. Increasing hardenability by adding Boron does not decrease the Ms temperature.

These arise because of the manner in which B produces its effect and the interactions of Boron with other elements in steel. To be effective, Boron must be in solid solution in austenite. The solubility of Boron in austenite is very low, for example, the solubility at 912 °C is about 0.001 wt. %, increasing with temperature to a maximum value of about 0.005 wt. % at the eutectic. In -iron, the solubility is essentially zero, but is influenced by the impurities present. Because of its low solubility in austenite, Boron can be highly concentrated in grain boundaries.

When boron steel is cooled from the hardening temperature the solubility of boron is reduced, which results in a still greater concentration of Boron at the grain boundaries. The presence of boron in solid solution and coherent boron carbide in the grain boundaries delays

the formation of ferrite and pearlite and to some extent, bainite; hence increasing the hardenability of the steel (Thelning,1984).

The effect of Boron may be expressed quantitatively as the boron factor, which is the ratio of the ideal diameters, D_i, (according to Grossmann) for the steel with and without boron, viz.

$$B_f = \frac{D_i \; with \; Boron}{D_i \; without \; Boron}$$

Di (with boron) is derived from the Jominy end-quench hardenability curve; Di (without boron) is calculated from the chemical composition of the steel.

The optimum Boron content as shown in the *Figure4.3* below, near 0.002 wt. %, for increasing hardenability in 0.2 % C, 0.65 wt. % Mn, 0.55 wt. % Mo steel is shown in figure below. Boron contents above about 0.003 wt. % lead to a loss in hardenability, and Boron more than about 0.004 wt. % causes a loss in toughness through precipitation of Fe_2B in austenite grain boundaries (Leslie,1981)

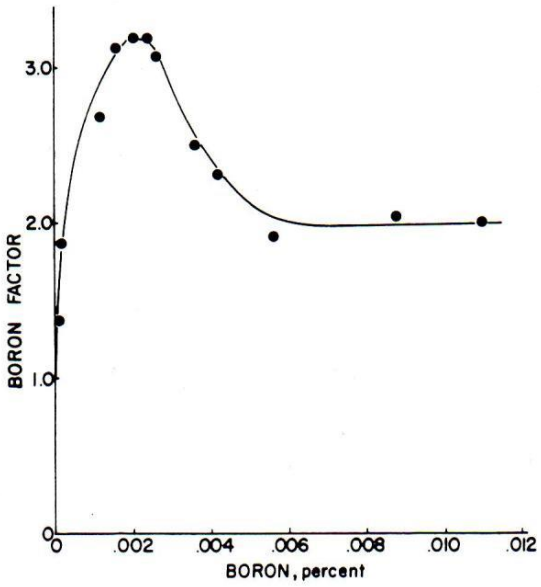

Figure 4.3 Boron hardenability factor as a function of boron content in a 0.20 wt. % C, 0.55% Mo, 0.65% Mn steel. (Leslie,1981)

5 MATERIALS AND METHODS

A layout shown in the *Figure 5.1* is followed up with the discrete overview of the process to be carried from start to the end of the process.

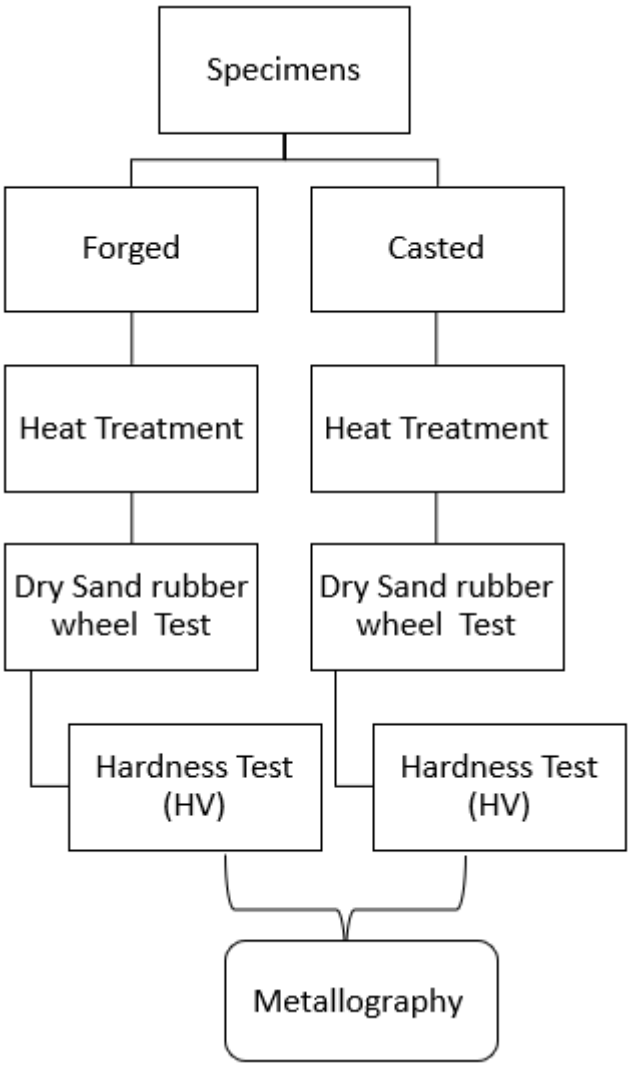

Figure 5.1 Experimental procedure layout for abrasive wear test

5.1 EXPERIMENTAL PROCEDURE AND MATERIAL:

The experimental procedure was carried out by using three body abrasive wear teat using rubber wheel, ASTM G 65. Iron alloys were casted in an induction furnace in the Czech Technical University in Prague (CTU) and Czech University of Life Sciences (CULS), Faculty of Engineering, Department of Material Science and Manufacturing Technology's Laboratory.

Abrasive wear tests on the casted alloys and the forged alloys of similar composition were conducted in (CULS), Faculty of Engineering, Department of Material Science and Manufacturing Technology's Laboratory.

5.2 MATERIAL:

The steel alloys were manufactured in CTU. The chemical composition of the specimens is listed below in the *Table 5.1*.

Table 5.1 Chemical composition of the Specimens

Exp / Pr	Wt.% B	Wt.% C	Wt.% Nd	Wt.% Cr
E71K1	0.6	0.52	0	0.2
E82K1	0.6	0.52	0.4	1

Casted and forged specimens were cut off from large billet into smaller cut in the laboratory using versatile tabletop cut-off machines Discotom-10 manufactured by Struers GmbH. Thereafter, the smaller cut was turned into test specimens by surface treatment. The specimens were grinded until they the met the ASTM 65 (shown in the *Figure 5.2*) standard size (25 mm x 10 mm x 50 mm)

Prior to heat treatment, protective paint of Condursal Z1100 was applied to the specimens for protection against oxidation and scaling during austenitizing and annealing with oxygen present. The furnace was heated for 5 hours to maintain temperature before the heat treatment initiated. The specimens were heat treated to 900 °C for 30 minutes. It was then passed to Salt Bath (mixture of KNO_3 50-60 % and $NaNO_3$ 50-60%) furnace for 2 hours for 2 hours.

After heat treatment the specimen were water cooled as it changes the were cooled for cleaning salt from the surface of the specimens. The alloys were then cleaned by grounding to attain the required ASTM G 65-93 standards.

Figure 5.2 Standard test machine for measuring abrasion using the dry sand/rubber wheel device (ASTM G65), CULS, Faculty of Engineering, Department of Material Science and Manufacturing Technology's Laboratory.

5.3 ABRASIVE WEAR TEST

Purified quartz sand of size 0.2 mm – 0.315 mm is mounted in the hopper. The amount is sand is calculated as per the timeframe of the revolution of the wheel. The sands are gravity fed from the hopper and interact with the rubber wheel and the test specimens it's shape is inclined, and the sand particles ranges from 212 µm to 300 µm as specified by the ASTM standards (ASTM G 65-00, 2000).

The sand particles get trapped in between the sample and a rubber wheel as it rotates. The sample is held against the wheel with a contact force as this type of wear is slow, field marks alone would be slow for the evaluation of new materials. The friction between the pressed sample and sand leads to removal of small number of particles from the sample. Dry sand rubber wheel abrasive wear test is a quick and cost-effective way to obtain vast amounts of information on wear rates and wear mechanisms and provides and provides an adequate correlation with the field test and has been used for several years by various laboratory (Hawk et all, 2016).

5.3.1 HARDNESS TEST (VICKER'S HARDNESS TEST)

The Vickers's hardness test as shown in the *Figure 5.3* is the most accurate and has continuous scale of hardness.

Figure 5.3 Vickers's Hardness Test in Laboratory of CULS, Faculty of Engineering, Department of Material Science and Manufacturing Technology

Vicker's test as show below in *Figure 5.4* is very suitable for hardened material due to small impression made on the sample while testing.

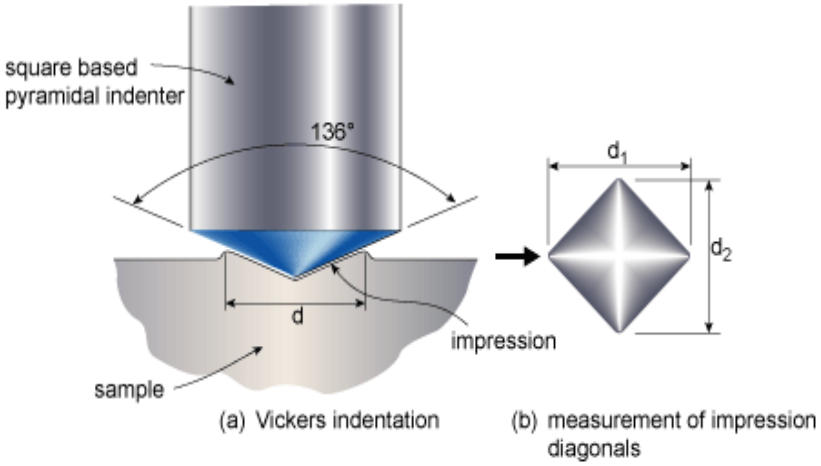

Figure 5.4 Schematic diagram of Vickers's Hardness test (ASTM E92-16, 2016)

5.4 METALOGRAPHY

After wear test specimens were cut and were casted by resin mould. After the mould set, it was grinded by MD Piano 220 and MD Allegro with 9 µm diameter suspension with lubricants in Tegramin -30 manufactured by Struers. Sample as then lapped with MD Dac 3 µm diameter and polished with the aid of MDchem and suspension of aluminum oxide (Al_2O_3). After this the hardness of the microstructure was determined with HV 5/ 125 for all specimens for the statistical calculation. The polished specimens were chemically etched by the aid of Nital (HNO_3 in ethanol) in order to provide light and smooth surface with better contrast between, the metal matrix and carbide for the structural configuration with the optical microscope (ARTCAM 300MI). Quantitative image analysis was carried out by Jenavert Microscope PA HD for characterizing the microstructure of matrix-carbide composition and the particle detection occurred automatically for the predefined gray-value needing, in some cases manual adjustment was carried out. The setup apparatus is shown in the *Figure 5.5* below

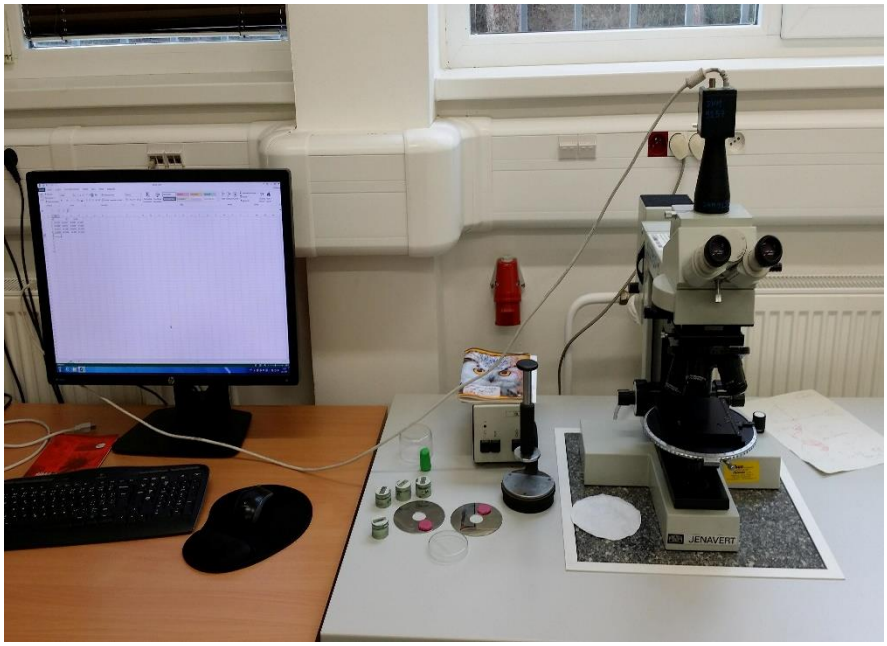

Figure 5.5 ARTCAM 300MI Microscope and Jenavert Microscope PA HD connected with a PC in Laboratory of CULS, Faculty of Engineering, Department of Material Science and Manufacturing Technology

6 RESULTS AND DISCUSSION

6.1 RESULTS OF WEAR LOSS

Experimental results include abrasion wear testing and microstructural observation. An abrasive wear test was performed on the dry rubber wheel test (ASTM G-65) to measure the wear properties expressed in wear rates for various alloys tested and the result tables are presented in the appendix.

The measured mass loss was used by weighing the sample before in an electronic balance with an accuracy of 0.001 g and the relative wear rate, expressed as a ratio of the mass loss of the sample to that of the reference material. The microstructural examination of the sample, the worn surface, the substrate was used to show the wear mechanism in terms of wear resistance versus microstructural properties. This study was carried out using scanning electron microscopy and the impact on the wear rate of the operating variables of the shifting speed of the load thus applied and the wear direction tested by the mass loss of all samples of the materials were measured and tabulated as shown below in *Table 6.1*.

Table 6.1 Results of Mean, Median, Standard Deviation and Relative Error of Mass Loss Samples

S. N	Sample	Median	Mean	Standard Deviation	Relative error
1	E82K1	0.010	0.010	0.001	8.40%
2	E71K1	0.014	0.014	0.001	8.90%
3	E82K1S	0.013	0.013	0.002	12.40%
4	E71K1S	0.011	0.010	0.001	8.30%

Specific abrasion wear loss is calculated by following *Equation 3*. The abrasive wear depends on the particle shape and size, hardness and the magnitude of the normal load applied to the particle and abrasive particles frequency of contact. Loss of weight of the specimens signifies the wear resistance. Lower volume loss is found in the materials which possess higher abrasion resistance (Agarwal et all, 2013).

$$W_s = \frac{\Delta V}{F_n \, X \, S_n} \qquad \text{(eq.3)}$$

W_s specific wear rate $(m^3.N^{-1}.m^{-1})$

ΔV is a mass loss (g)

F_n is an applied load (N)

S_n is a sliding distance (m)

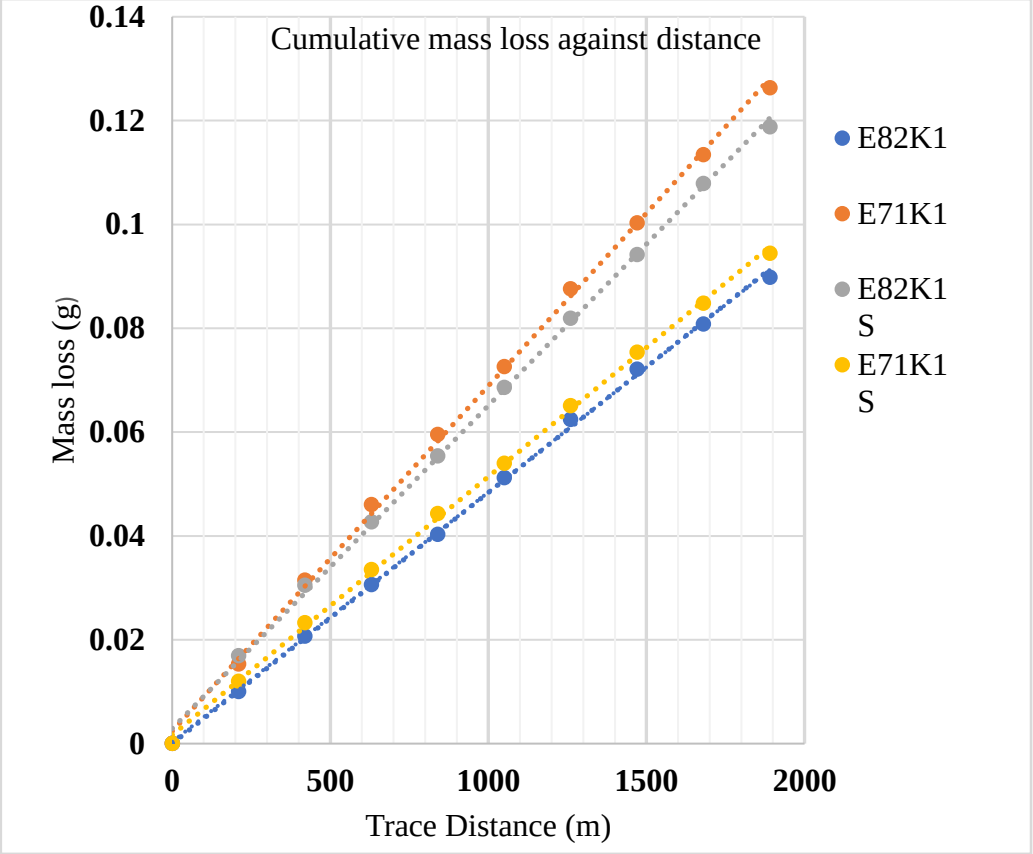

Figure 6.1 Cumulative mass loos against distance.

Above *Figure 6.1* shows the graph of cumulative mass loss against distance.

Table 6.2 Fits for all sample distances.

Sample Specimen	Fits Line	R^2
E82K1	$4.81.10^{-5}.x$	0.99
E71K1	$6.22.10^{-5}.x$	0.99
E82K1S	$6.65.10^{-5}.x$	0.99
E71K1S	$4.97.10^{-5}.x$	0.99

Where x is a distance

Table 6.2 above shows the fits for all sample distances.

6.2 STATISTICS

The data recorded in the experiment were subjected to analysis of variance (ANOVA). F-critical were calculated from the standard errors of the difference of the means. Statistical significance was set at $p<0.05$. All graph and table were plotted using Microsoft Excel 2016.

We have total 9 observations and after regression analysis run our R-square value is 0.688, which means model has been explained by 68.8%. This also says that the model has been highly fit.

Another most important part of the above table is F-test, which tells about the significance of the model.

We have,

If F value > α value = significant

If F value < α value = insignificant

Where,

Significant level (α) = 0.05

F-value = 2.207

Or, F > α = model significant

Or, 2.207 > 0.05 = model significant

Since our model has higher "F" value than α value, it represents our model is significant.

Statistical analysis is carried out via F test of slope as shown in the *Table 6.3* to figure out the sample's wear loss and its goodness of fit. After this test the result is read, and discussion is placed forward with the case and effect of the outcome from the analysis done.

Table 6.3 Statistical analysis of wear loss for sample specimen – F test of slope.

SUMMARY OUTPUT	
Regression Statistics	
Multiple R	0.83
R Square	0.688
Adjusted R Square	0.376
Standard Error	454.198
Observations	9

It means that the slope has been explained by almost 69% of wear loss, also while checking the goodness of fit this value represent model is highly fit.

ANOVA

	df	*SS*	*MS*	*F*	*Significance F*
Regression	4	1820818	455205	2.207	0.231
Residual	4	825182	206295		
Total	8	2646000			

Since, F value is greater than alpha value or significant level (0.05), model is significant.

	Coefficients	*Standard Error*	*t Stat*	*P-value*
Intercept	7017.819	2233.587	3.142	0.035
E82K1	-58639.746	235409.753	-0.249	0.816
E71K1	-172834.58	223498.23	-0.773	0.482
E82K1S	-81030.954	135235.672	-0.599	0.581
E71K1S	-179968.59	352537.183	-0.51	0.637

6.3 RESULT AND DISCUSSION

Statistical analysis carried in *Table 6.*3 shows that the wear rate of specimens decreases with increase in of boron content in the alloy. E71K1S and E82K1 were remarkably recorded with low wear rate due to the close proximity of the boron concentration, which strongly influenced the hardness and wear resistance of the materials during the tests. E71K1 and E82K1 recorded the highest wear rate due to the low boron content in the material.

In addition, the E82K1 test listed a negligible wear rate due to the proximity of the boron content, which made it harder and more resistant to wear depending on the quality of the structure and the network organization and dispersion of carbide stages. Therefore, E82K1 followed by E71K1S seems with more significance than the E71K1 and E82K1S.The most significant seems to be E82K1 and the least sems to be E71K1.

E82Kl and E82KlS contains high amount of Cr. 1.0 wt.% than the E7lKl and E71K1S which contains only 0.2 wt.%. In similar way E82Kl and E82K1S contains 0.4 wt.% of Nd whereas E71Kl and E71KlS have no traces of Nd at all. Cr replaced carbide.in high chromium cast

alloy. Both calculated and simulated (F-test) formulated the same results with respect to durability of abrasive wear resistance.

Moreover, samples E71K1S and E82K1S were treated in salt bath furnace whereas E71K1 and E82K1 were not. E71K1 and E82K1 were casted whereas E71K1S and E82K1S were forged annealed. Although, E71K1S achieved lower abrasive resistance than E82K1S which was treated in the salt bath. E82K1 showed the lowest abrasive, which was not treated with the salt bath, but it was forged annealed.

E82K1 turned out be the best for the durability against abrasive wear without salt bath treatment. The most important facts for agricultural tools production are the cost of heat treatment. The morphology of the samples was very lightly altered in a wear test but not too much extent due to boron content in the samples. At the same time, the carbon content of the high chromium alloys is reduced to a level that reinforces the matrix, the boride having a hardness greater than that of the carbide.

The worn surface of the specimen was observed by Scanning Electron Microscopy (SEM) to determine the effect of increasing the sliding speed and distance, abrasive particle size and normal stress on the morphology of the worn surface of the samples. The most influence element on the microstructure was the element boron as seen from the metallography, *Chapter 6.4* as an alloying element and had a synergetic effect in the formation of borides. The microstructure is similar when compared to the other experiments that has already been done before this.

Similar experiment carried out by Sarfo (2017), in his master thesis concluded that the effect of increasing boron in the iron alloy materials plays important role in the hardness of the material. This result also corresponds with a research done my Budhely et al (2005) on abrasive wear of hard facing alloys. The outcome of this method thus conducted on the steel was high hardness, improved fatigue resistance and good wear resistant.

Heat treatment is one of the special aspects of the desired properties of the material, microstructure was detected by abrasive wear mechanisms wear micro grooving and fatigue

shown in the fractography of worn surfaces *Chapter 6.5* which is commonly present as an abrasive wear in the agricultural tools.

The main advantage of high-born iron alloys its relatively cheap and uses lower alloying traditional elements like Cr, Nd, Ti and other. Even with utilization of lower traditional alloying element we can produce higher qualify of iron alloys just by addition of small amount of boron as of the alloying element.

Agricultural machinery is continuously adapting to new knowledge and farmers demand for tools with better too wear on their machines. Steady development and monitoring of the agricultural tools is the essential part for designing the agricultural too machinery.

6.4 METALLOGRAPHY

Metallography of Sample E71K1 and E82K1

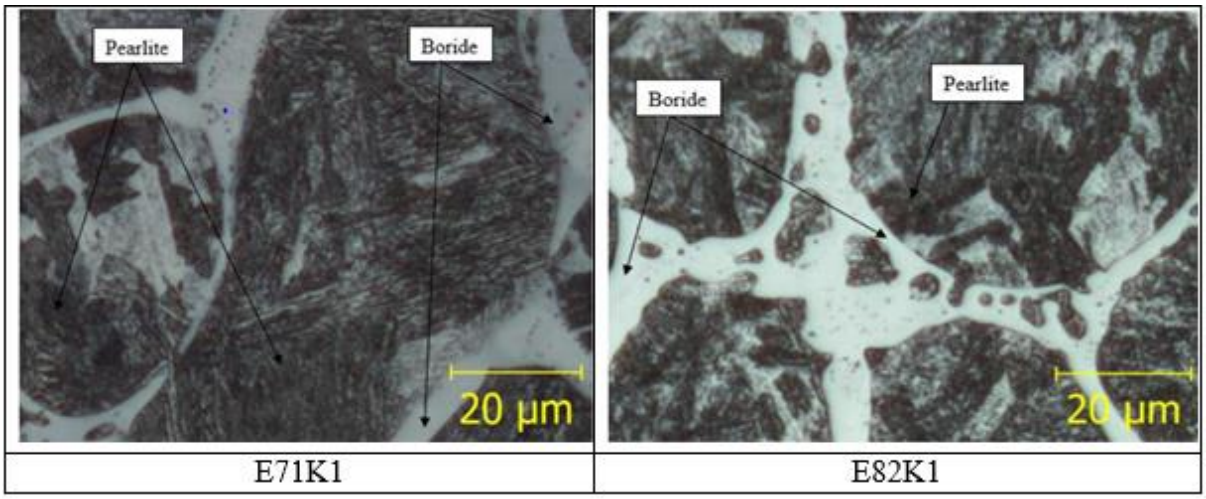

Figure 6.2 Light Optical microstructure analysis of casted specimen E71K1 (0.6 wt. % B).

Above *Figure 6.2* shows Light Optical microstructure of cast specimens with 0.6 wt. % B of boron addition. The microstructure analysis shows that E82K1 has higher volume of pearlite than other samples of E71K1. It is observed that the chromium increased volume of pearlite and E82K1 and E71K1 has higher volume of pearlite than other samples.

Metallography of Sample E82K1S and E71K1S

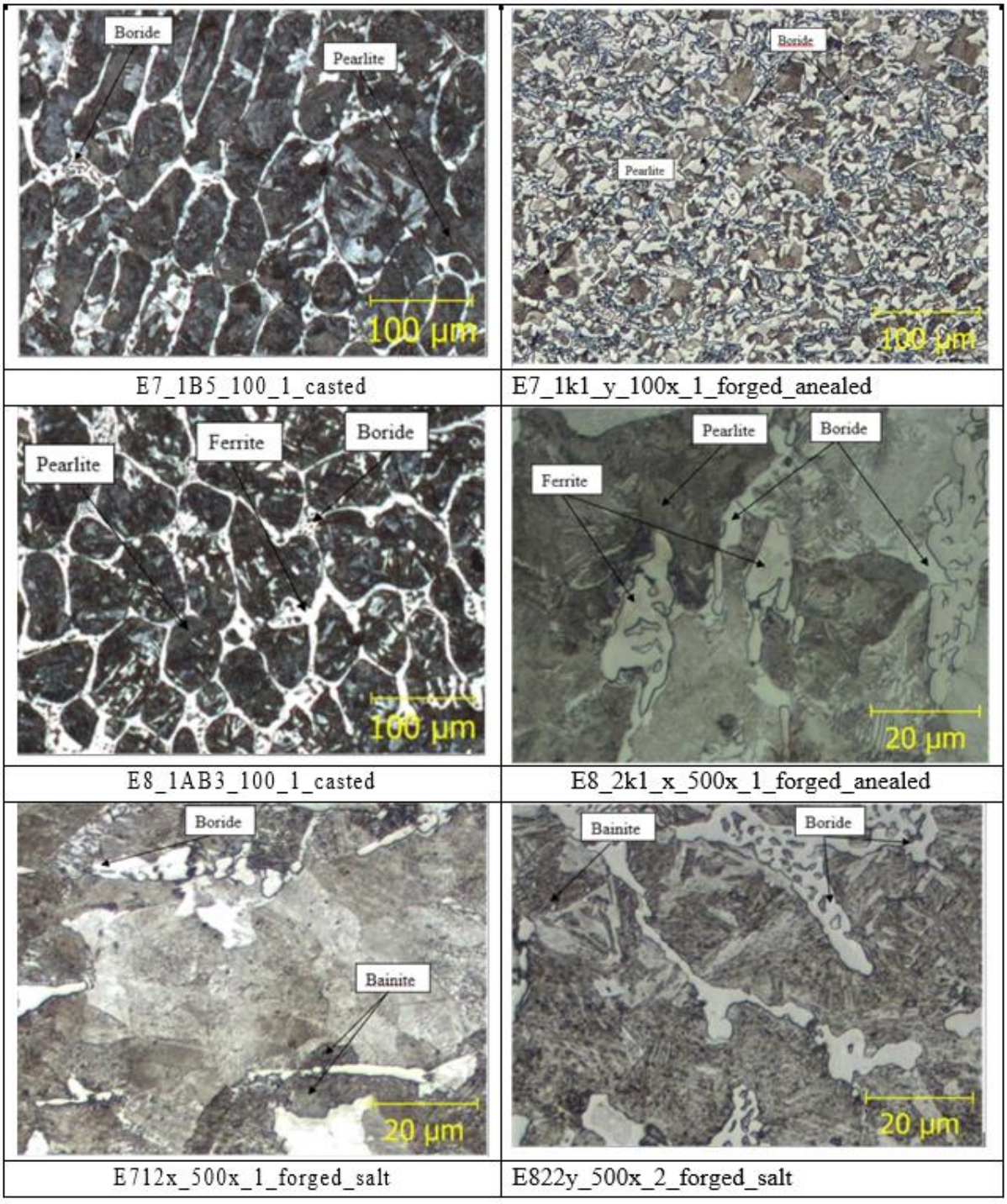

Figure 6.3 Light Optical microstructure analysis of casted specimen E82K1 (0.6 wt. % B).

Above *Figure 6.3* shows Light Optical microstructure analysis of cast specimens with (0.6 wt. % B) boron addition. The microstructure analysis shows that the sample E8_1AB3_500_1 has higher volume of pearlite than other samples of E81K1. It is seen that chromium increased volume of pearlite and E8_1AB3_500_3 and E8_1AB3_500_1 has higher volume of pearlite than other samples.

The microstructure of specimens shows that the sample E7_1k1_y_100x_1_forged_anealed has higher volume of boron than other samples of E8_2k1_x_500x_1_forged_anealed. It is seen that almost same consistency of boron, ferrite and pearlite in the sample E7_1B5_100_1_casted and E8_1AB3_100_1_casted.

Sample E712x_500x_1_forged_salt and E822y_500x_2_forged_salt contains less borides and more bainite with no presence of pearlite. The salt bath treatment has wide operating temperature range. G.P. Dubal in 1999 quoted that salt bath causes less distortion and produces uniform and consistent hardness.

6.5 FACTOGRAPHY OF WORN SURFACES

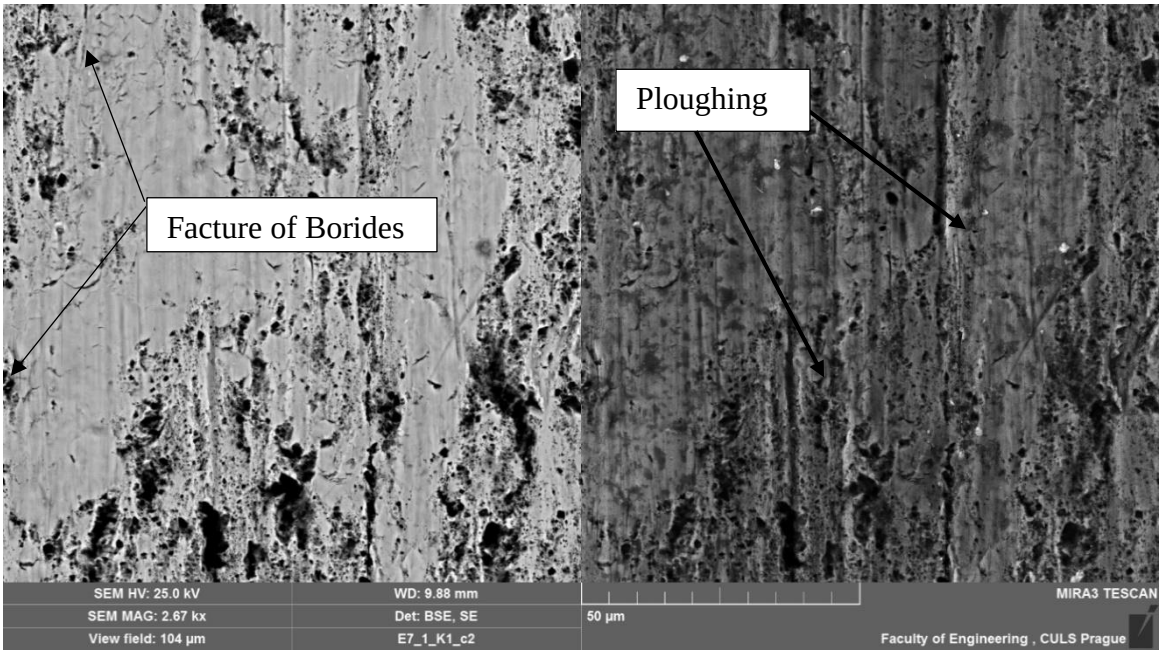

Figure 6.4 Worn surface of E71K1: Left BSE (Back scattered electron), Right SE (secondary electron).

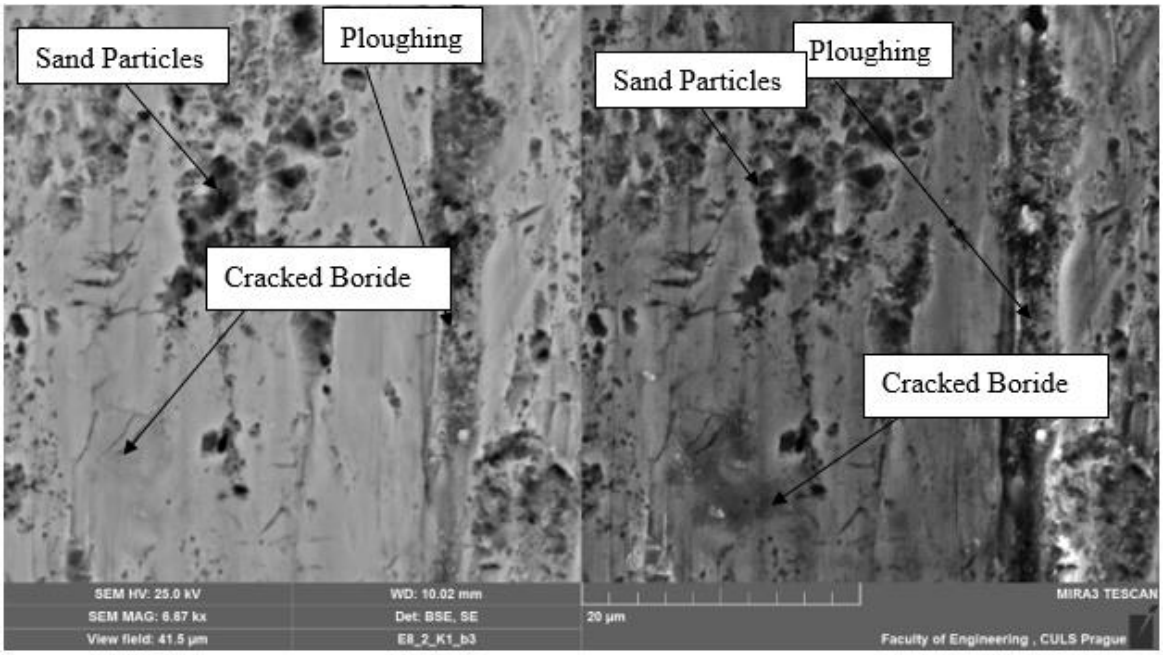

Figure 6.5 Worn surface of E82K1: Left BSE (Back scattered electron), Right SE (secondary electron).

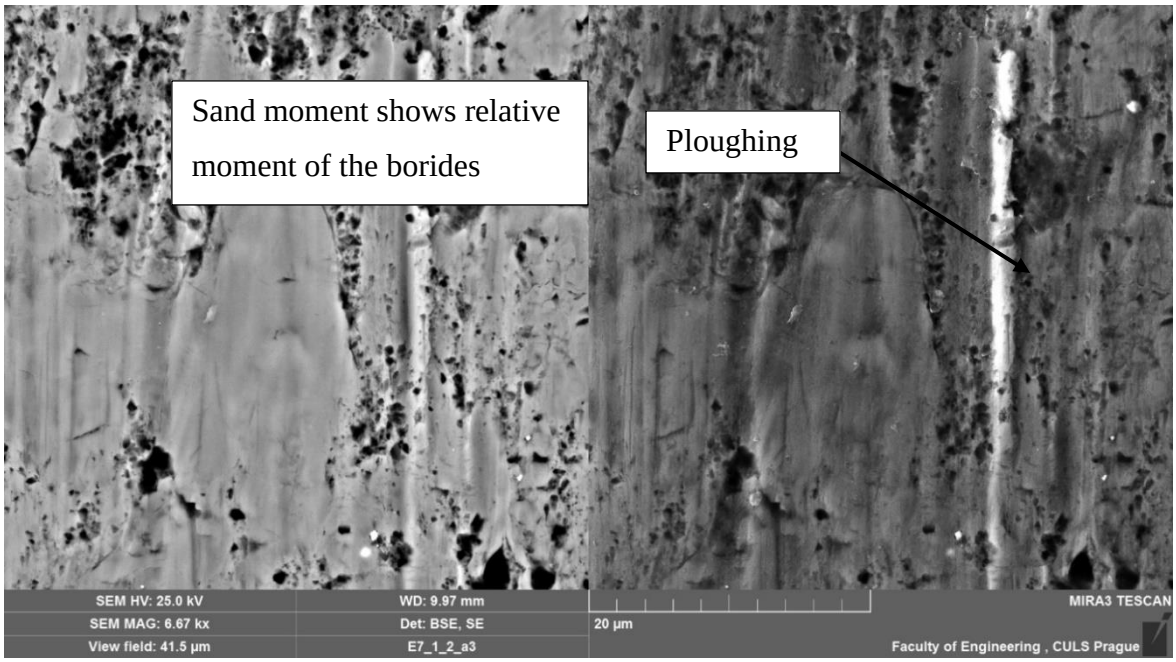

Figure 6.6 Worn surface of E71K1S: Left BSE (Back scattered electron), Right SE (secondary electron).

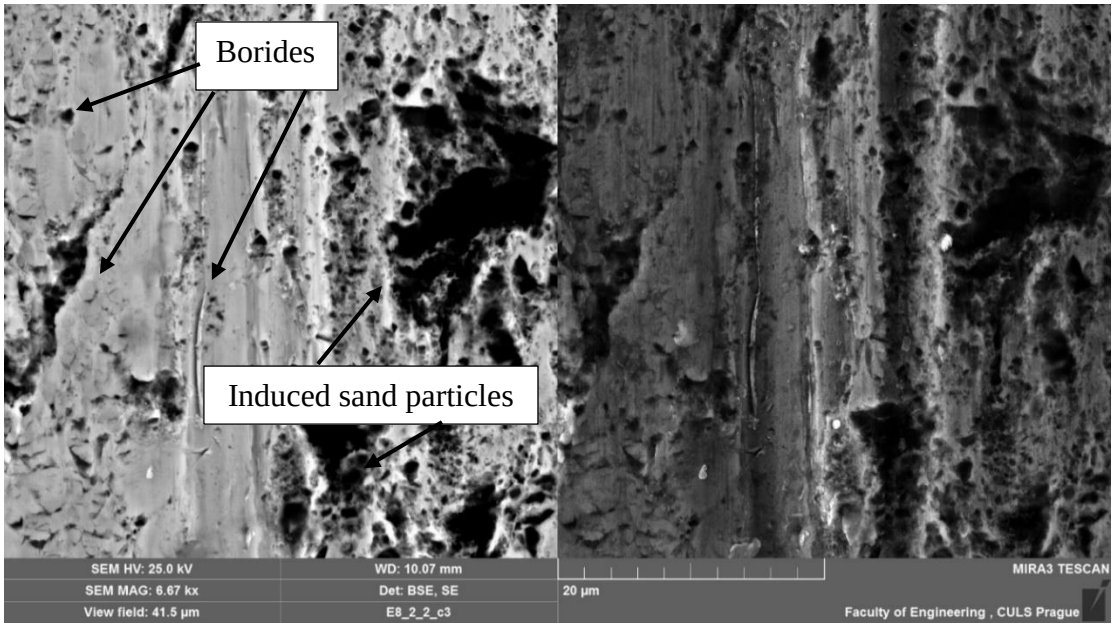

Figure 6.7 Worn surface of E71K1S: Left BSE (Back scattered electron), Right SE (secondary electron).

The fractography of samples from *Figure 6.4-6.7* is described as follows:

1. Sample E71K1 in fractography shows that the wear mechanism of matrix is different from that of wear mechanism of borides. It was observed that borides cracked according to mechanism C in figure 10 and matrix is worn in the process of ploughing.
2. Sample E82K1 shows the same mechanism as sample E71K1. Both samples were casted.
3. Sample E71K1S is forged annealed and treated with salt bath furnace shows that the wear mechanism of matrix is different from that of wear mechanism of borides, similar to sample E71K1. It is visible that fewer borides are cracked according to mechanism C in figure 10, but borides samples are better in ploughing than samples E71K1, E82K1 and E82K1S, also the matrix is worn while ploughing and it always indicates interaction of particles and matrix, F in figure 10.
4. Sample E81K1S is also forged annealed and treated with salt bath furnace shows the same mechanism as sample E71K1.
5. Samples in appendix 2 follows similar mechanism as that of sample E71K1.
6. Samples in appendix 3 follows similar mechanism as that of sample E71K1.
7. Samples in appendix 4 follows similar mechanism as that of sample E71K1S.
8. Wear loss result and fractography of samples are corelated. Similar result is obtained from the both.

7 CONCLUSSION

Abrasive wear test was conducted on four specimens of iron alloy materials with different chemical composition using the dry sand rubber wheel test (ASTM G-65). First 2 tested samples were casted, and rest were forged.

All samples were heat treated but the last 2 samples were passed through Salt Bath furnace

Results thus identified are as follows:

1. Hardness and strength of the material were found to increases with increasing the boron concentration to resist the wear.
2. Wear rate decreased with the increment in the boron content and increase in the boron content in decreases the toughness of the material which increases its hardness in turn to withstand the wear.
3. Fractography of the samples showed the increment in the boron content increases the boride's microstructure, which increases the materials properties to resist wear.
4. Boron along with proper heat treatment played the vital role in the reinforcement of the hardness.
5. E71K1 and E82KlS were found to be the most feasible samples for the usage as possess lower wear rate which means they last longer and need not be replaced earlier than the other samples with higher wear rate.
6. It is also observed that the forged annealed salt bath treated samples performed better than the samples that were casted.
7. E71KIS was found to be most feasible and promising sample with lowest wear rate as form the F-test of slopes of the tested samples.
9. Microstructural analysis showed an interaction of boron with matrix alloying elements. The formation of borides caused the increase of microhardness and hardness values of matrix. The higher density and microhardness expressed in higher strength of material

8 BIBLIOGRAPHY:

1. Furtado, H.S., Bernardes, A.T., Machado, R.F. and Silva, C.A., 2011. The effect of adding boron in solidification microstructure of dilute iron-carbon alloy as assessed by phase-field modeling. *Materials Research, 14(2)*, pp.195-205.
2. Bialon, A., 2013. *The Iron-Boron System: Ordered Structures and Point Defects* (Doctoral dissertation).
3. Ivanovskii, A.L., 2012. Mechanical and electronic properties of diborides of transition 3d–5d metals from first principles: Toward search of novel ultra-incompressible and superhard materials. *Progress in Materials Science*, *57*(1), pp.184-228.
4. Gu, Q., Krauss, G. and Steurer, W., 2008. Transition metal borides: superhard versus ultra-incompressible. *Advanced materials*, *20*(19), pp.3620-3626.
5. Kaner, R.B., Gilman, J.J. and Tolbert, S.H., 2005. Designing superhard materials. *Science*, 308(5726), pp.1268-1269.
6. Gilman, J.J., Cumberland, R.W. and Kaner, R.B., 2006. Design of hard crystals. *International Journal of Refractory Metals and Hard Materials*, 24(1-2), pp.1-5.
7. Levine, J.B., Tolbert, S.H. and Kaner, R.B., 2009. Advancements in the search for superhard ultra-incompressible metal borides. *Advanced Functional Materials*, *19*(22), pp.3519-3533.
8. Jiménez, J.A., González-Doncel, G. and Ruano, O.A., 1995. Mechanical properties of ultrahigh boron steels. *Advanced Materials*, 7(2), pp.130-136.
9. WATANABE, S. and OHTANI, H., 1983. Precipitation behavior of boron in high strength steel. *Transactions of the Iron and Steel Institute of Japan*, *23*(1), pp.38-42.
10. WATANABE, S., OHTANI, H. and KUNITAKE, T., 1983. The influence of dissolution and precipitation behavior of M23 (C, B) 6 on the hardenability of boron steels. *Transactions of the Iron and Steel Institute of Japan*, *23*(2), pp.120-127.
11. Sudo, A., Nishi, T., Shirasu, N., Takano, M. and Kurata, M., 2015. Fundamental experiments on phase stabilities of Fe–B–C ternary systems. *Journal of Nuclear Science and Technology*, *52*(10), pp.1308-1312.
12. Thevenot, F., 1991. A review on boron carbide. *In Key Engineering Materials* (Vol. 56, pp. 59-88). Trans Tech Publications Ltd.
13. Zum Gahr, K.H., 1987. *Microstructure and wear of materials* (Vol. 10). Elsevier.

14. Pertek, A. and Kulka, M., 2003. Characterization of single tracks after laser surface modification of borided 41Cr4 steel. *Applied Surface Science, 205*(1-4), pp.137-142.
15. Mazahery, A. and Shabani, M.O., 2012. Study on microstructure and abrasive wear behavior of sintered Al matrix composites. *Ceramics International, 38*(5), pp.4263-4269.
16. Li, C., Shen, B., Li, G. and Yang, C., 2008. Effect of boronizing temperature and time on microstructure and abrasion wear resistance of Cr12Mn2V2 high chromium cast iron. *Surface and Coatings Technology*, *202*(24), pp.5882-5886.
17. Yi, D., Xing, J., Ma, S., Fu, H., Chen, W., Li, Y., Yan, J., Zhang, J., Liu, Z. and Zhu, J., 2011. Three-body abrasive wear behavior of low carbon Fe–B cast alloy and its microstructures under different casting process. *Tribology Letters*, *42*(1), pp.67-77.
18. Lakeland, K.D., Graham, E. and Heron, A., 1992. Mechanical properties and microstructures of a series of FCB alloys. *The University of Queensland, Brisbane, Australia*, pp.1-13.
19. Ma, S., Xing, J., Yi, D., Fu, H., Liu, G. and Ma, S., 2010. Microstructure and corrosion behavior of cast Fe–B alloys dipped into liquid zinc bath. *Materials characterization*, *61*(9), pp.866-872.
20. Ma, S., Xing, J., Fu, H., Yi, D., Li, Y., Zhang, J., Zhu, B. and Gao, Y., 2012. Microstructure and interface characteristics of Fe–B alloy in liquid 0.25 wt.% Al–Zn at various bath temperatures. *Materials Chemistry and Physics*, *132*(2-3), pp.977-986.
21. Lu, Y., 2007. *Effect of Boron on Microstructure and Mechanical Properties of Low Carbon Microalloyed Steels* (Doctoral dissertation, McGill University Montreal, Canada).
22. Morral, J.E. and Cameron, T.B., 1977. A model for ferrite nucleation applied to boron hardenability. *Metallurgical Transactions* A, 8(11), pp.1817-1819.
23. Lu, Y., 2007. *Effect of Boron on Microstructure and Mechanical Properties of Low Carbon Microalloyed Steels* (Doctoral dissertation, McGill University Montreal, Canada).
24. Guttmann, M., McLean, D., Johnson, W.C. and Blakely, J.M., 1979. Interfacial segregation. *ASM, Metals Park, Ohio*, 261.

25. Shen, X.P. and Priestner, R., 1990. Effect of boron on the microstructure and tensile properties of dual-phase steel. *Metallurgical transactions A, 21*(9), pp.2547-2553.
26. Yi, D., Xing, J., Ma, S., Fu, H., Chen, W., Li, Y., Yan, J., Zhang, J., Liu, Z. and Zhu, J., 2011. Three-body abrasive wear behavior of low carbon Fe–B cast alloy and its microstructures under different casting process. *Tribology Letters, 42*(1), pp.67-77.
27. Spiridonova, I.M., 1984. Structure and properties of iron-boron-carbon alloys. *Metal Science and Heat Treatment, 26*(2), pp.170-174.
28. Filonenko, N.Y., Beryoza, O.Y. and Bezrukava, O.G., 2013. The effect of carbon on phase composition and phase transformations in Fe-B system alloys. *Promblems of atomic science and technology*, (5), pp.168-172.
29. Sukhovaya, E. V. "Structural approach to the development of wear-resistant composite materials." *Journal of Superhard Materials 35*, no. 5 (2013): 277-283.
30. Załuska, A. and Matyja, H., 1983. Crystallization characteristics of amorphous Fe-Si-B alloys. *Journal of materials science, 18*(7), pp.2163-2172.
31. Spiridonova, I.M., Sukhovaya, E.V. and Sergeev, G., 2006. Phase transformations in high-boron carbon alloyed iron alloys. Theory and practice of metallurgy. Special Edition. *Eutectica VII, 4*(53-54), pp.57-59.
32. Kuzma, Y.B. and Chaban, P.F., 1990. Boron-bearing binary and ternary systems. Handbook. Moscow. *Metallurgy.*
33. Samsonov, G.V., Serebryakova, T.I. and Neronov, V.A., 1975. Borides; *Boridy*.
34. Voa, A.E. and Kagan, I.K., 1976. *Structure and properties of binary metal systems*.
35. Baklanov, D.A., Vnukov, I.E., Zhandarmov, Y.V. and Shatokhin, R.A., 2010. Structure estimates of crystalline specimens by means of fast electrons emission in these specimens. *Surface. X-ray, synchronous and neutron investigations*, (4), p.7.
36. Podolinsky, V.V., Taran, Y.N. and Drykin, V.G., 1989. Classification of binary eutectics. *Journal of crystal growth, 96*(2), pp.445-449.
37. Lv, Z., Fu, H., Xing, J., Ma, S. and Hu, Y., 2016. Microstructure and crystallography of borides and mechanical properties of Fe–B–C–Cr–Al alloys. *Journal of Alloys and Compounds*, 662, pp.54-62.
38. Röttger, A., Lentz, J. and Theisen, W., 2015. Boron-alloyed Fe–Cr–C–B tool steels—Thermodynamic calculations and experimental validation. *Materials & Design*, 88, pp.420-429.

39. Borisov, Y.S., Oliker, V.E., Astakhov, E.A., Korzhik, V.N. and Kunitskii, Y.A., 1987. Structure and properties of gas-thermal coatings of Fe-BC and Fe-Ti-BC alloys. *Soviet Powder Metallurgy and Metal Ceramics, 26*(4), pp.313-318.
40. Föll, H., Iron, Steel and Swords script, Chapter: Thermal and Residual Stress, retrieved on 12.12. 2016.
41. ASTM G 65-00, 2000. Standard test method for measuring abrasion using the dry sand/rubber wheel apparatus *ASTM International, West Conshohocken, PA*.
42. Hawk, J.A., Wilson, R.D., Tylczak, J.H. and Doğan, Ö.N., 1999. Laboratory abrasive wear tests: investigation of test methods and alloy correlation. *Wear, 225*, pp.1031-1042.
43. ASTM E92-16, 2016. Standard test methods for vickers hardness and knoop hardness of metallic materials. *ASTM International West Conshohocken, PA*.
44. Safro, E, 2017. Abrasive wear of iron alloy, (Diploma dissertation, *Czech University of Life Sciences in Prague, Czechia*).
45. Moore, M.A., 1983. The effect of particle shape on abrasive wear: Comparison of theory and experiment. *Wear of materials, pp.1*-11.
46. Moon, O.M., Kang, B.C., Lee, S.B. and Boo, J.H., 2004. Temperature effect on structural properties of boron oxide thin films deposited by MOCVD method. *Thin Solid Films, 464*, pp.164-169.
47. Natsis, A., Papadakis, G. and Pitsilis, J., 1999. The influence of soil type, soil water and share sharpness of a mouldboard plough on energy consumption, rate of work and tillage quality. *Journal of Agricultural Engineering Research, 72*(2), pp.171-176.
48. Polak, R., Ilo, S. and Badisch, E., 2009. Relation between inter-particle distance (L IPD) and abrasion in multiphase matrix–carbide materials. *Tribology letters, 33*(1), pp.29-35.
49. Paju, M., Hougardy, H.P. and Grabke, H.J., 1989. Effects of Boron Alloying on the Properties of a Low-Carbon Low-Alloyed Steel. I. The Mechanical Properties. *Scand. J. Metall., 18*(5), pp.235-242.
50. Rabinowicz, E., Dunn, L.A. and Russell, P.G., 1961. A study of abrasive wear under three-body conditions. *Wear, 4*(5), pp.345-355.

51. Ribeiro, L., Barbosa, A., Viana, F., Baptista, A.M., Dias, C. and Ribeiro, C.A., 2011. Abrasion wear behaviour of alloyed and chilled cast irons. *Wear, 270*(7-8), pp.535-540.
52. Stachowiak, G.W. and Podsiadlo, P., 2001. Characterization and classification of wear particles and surfaces. *Wear, 249*(3-4), pp.194-200.
53. Scheffler, O. and Allen, C., 1988. The abrasive wear of steels in South African soils. *Tribology international, 21*(3), pp.127-135.
54. Weber, S. and Theisen, W., 2007. Sintering of high wear resistant metal matrix composites. *Advanced Engineering Materials*, *9*(3), pp.165-170.
55. Sen, S., Ozbek, I., Sen, U. and Bindal, C., 2001. Mechanical behavior of borides formed on borided cold work tool steel. *Surface and Coatings Technology*, *135*(2-3), pp.173-177.
56. Shackelford, J.F. and Clode, M.P., 2005. Introduction to materials science for engineers.
57. Avery, Howard S. "*Classification and precision of abrasion tests." Wear of Materials 1977. ASME, New York, N. Y. 1977, 148, 157* (1977).
58. Chung, R.J., Tang, X., Li, D.Y., Hinckley, B. and Dolman, K., 2013. Microstructure refinement of hypereutectic high Cr cast irons using hard carbide-forming elements for improved wear resistance. *Wear, 301*(1-2), pp.695-706.
59. Correa, R., Bedolla-Jacuinde, A., Zuno-Silva, J., Cardoso, E. and Mejía, I., 2009. Effect of boron on the sliding wear of directionally solidified high-chromium white irons. *Wear, 267*(1-4), pp.495-504.
60. Deuis, R.L., Subramanian, C. and Yellup, J.M., 1998. Three-body abrasive wear of composite coatings in dry and wet environments. *Wear, 214*(1), pp.112-130.
61. Leslie, W.C., 1981. The physical metallurgy of steels. *Hemisphere Publishing Corp., 1981*, p.396.
62. Axen, N. and Jacobson, S., 1994. A model for the abrasive wear resistance of multiphase materials. *Wear*, *174*(1-2), pp.187-199.
63. Yen, B.K. and Dharan, C.K.H., 1996. A model for the abrasive wear of fiber-reinforced polymer composites. *Wear*, *195*(1-2), pp.123-127.
64. Khrushchev, M.M. and Babichev, M.A., 1953. *Resistance to abrasive wear and the hardness of metals* (Vol. 15). US Atomic Energy Commission, Technical Information Service.

65. Agarwal, G., Patnaik, A. and Sharma, R.K., 2013. Parametric optimization and three-body abrasive wear behavior of sic filled chopped glass fiber reinforced epoxy composites. *International Journal of Composite Materials*, *3*(2), pp.32-38.
66. Buchely, M.F., Gutierrez, J.C., Leon, L.M. and Toro, A., 2005. The effect of microstructure on abrasive wear of hardfacing alloys. *Wear*, *259*(1-6), pp.52-61.
67. Chotěborský, R., Wear Resistant High Boron Steel for Agriculture Tools, 2019.

9 LIST OF ABBREVIATIONS AND SYMBOLS

µm	Micrometre
N	Newton
G	Grams
ASTM	American society for testing and materials
SEM	Scanning electron microscopy
Mm	Millimetre
A.C	Alternating current
CIAT	Continuous impact abrasive test
TIC	Titanium carbide
MMC	Metal metric composites
WC	Tungsten carbide
%	Percentage
B_2O_3	Boron trioxide
Ti	Titanium
V	Vanadium
Mo	Molybdenum
Nb	Niobium
W	Tungsten
Fe_2B	Iron boride
Fe-Cr-B	Boron solubility in cast iron
Cr	Chromium
M_7C_3	Primary eutectic carbide
$M_{23}C_6$	Hypereutectic carbide
TTT	Time temperature transformation
CCT	Continuous cooling transformation
FCC	Face cubic centre
BCC	Body cubic centre
Ni-hard 4	Medium alloy

APPENDIX 1

Distance	0	210	420	630	840	1050	1260	1470	1680	1890	2100
E82K1	92.7207	92.7079	92.6979	92.6872	92.6773	92.6676	92.657	92.6455	92.6358	92.6271	92.6181
E71K1	89.2844	89.2668	89.2515	89.2353	89.2208	89.2073	89.194	89.1792	89.1665	89.1534	89.1405

Cast

Distance	0	210	420	630	840	1050	1260	1470	1680	1890	2100
E82K1S	86.9612	86.9412	86.9243	86.9107	86.8985	86.8858	86.873	86.8593	86.847	86.8333	86.8224
E71K1S	87.0781	87.0593	87.0473	87.036	87.0258	87.015	87.005	86.9942	86.9839	86.9745	86.9649

APPENDIX 2

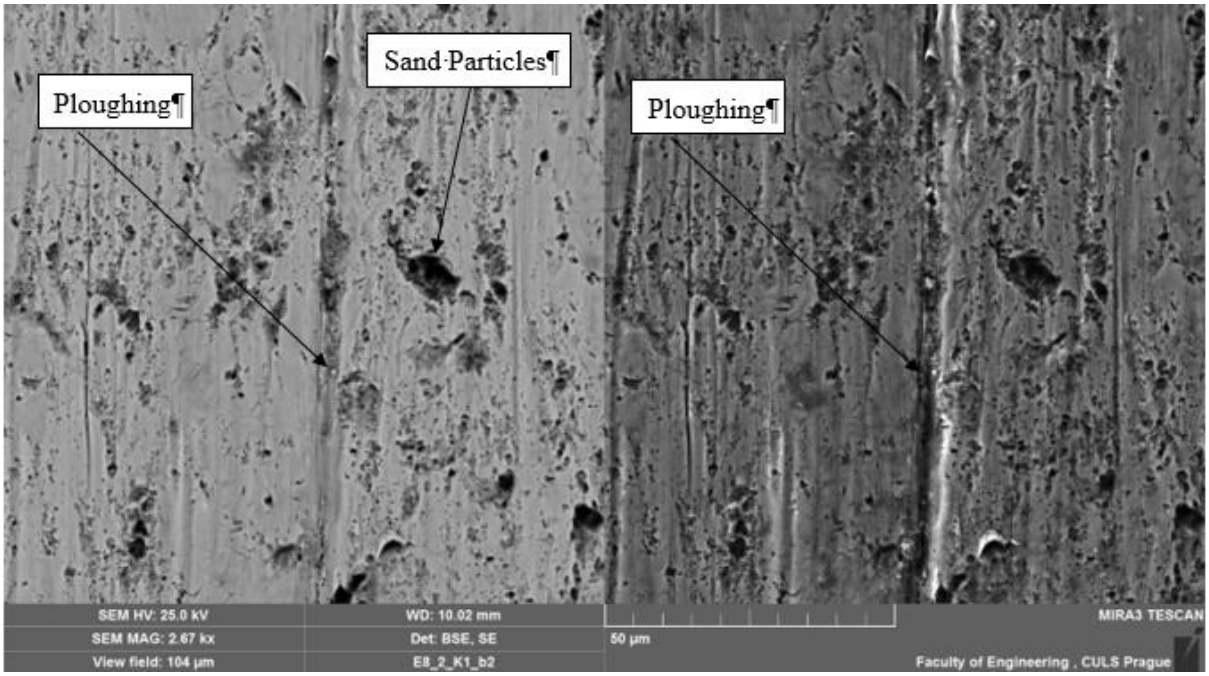

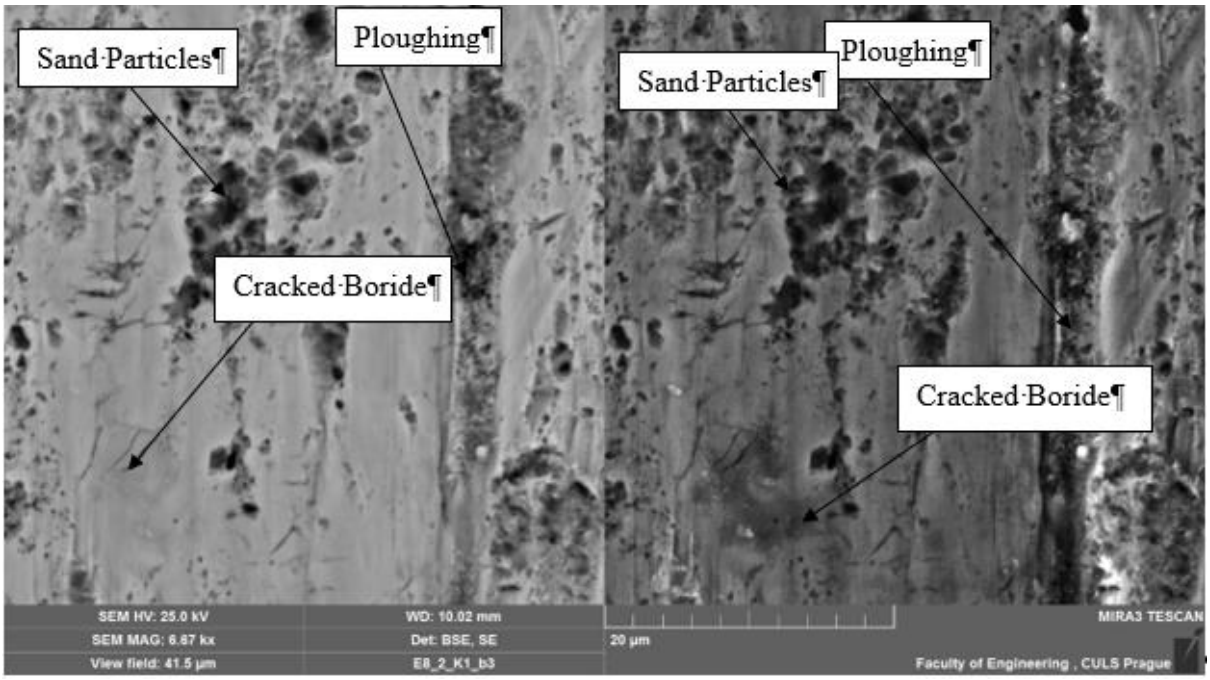
Sand·Particles¶
Ploughing¶
Cracked·Boride¶
Sand·Particles¶
Ploughing¶
Cracked·Boride¶
SEM HV: 25.0 kV
WD: 10.02 mm
SEM MAG: 6.67 kx
Det: BSE, SE
View field: 41.5 µm
E8_2_K1_b3
20 µm
MIRA3 TESCAN
Faculty of Engineering , CULS Prague

APPENDIX 3

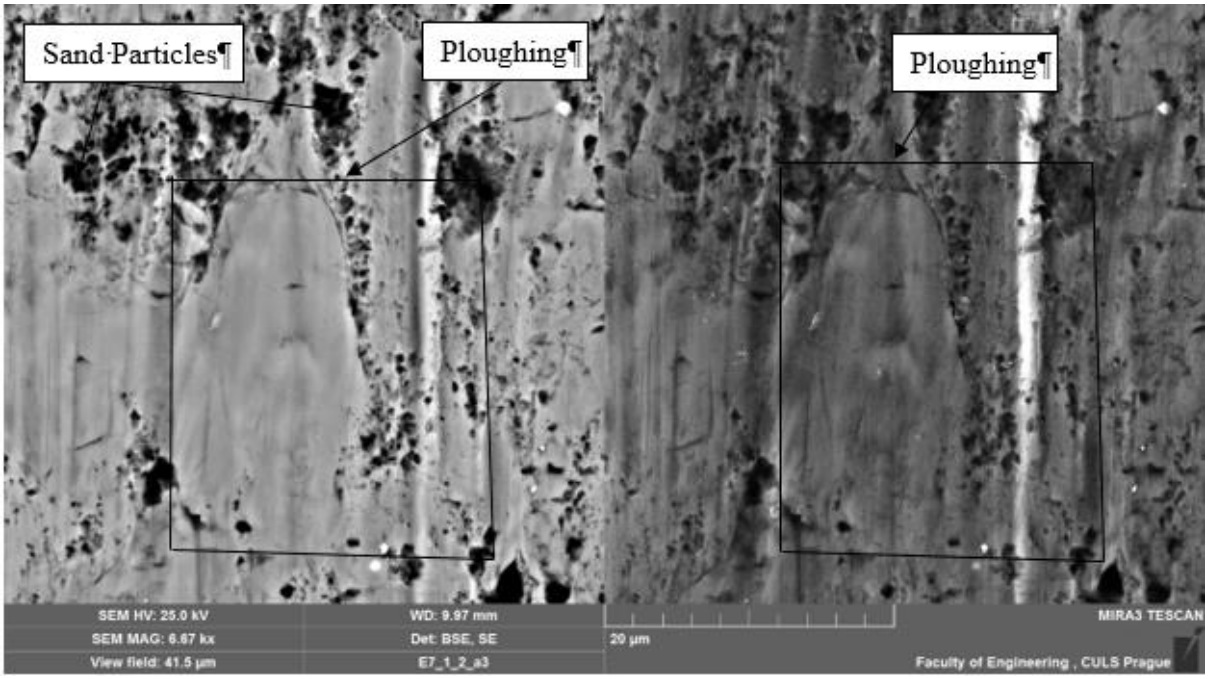
Sand·Particles¶
Ploughing¶
Ploughing¶
SEM HV: 25.0 kV
WD: 9.97 mm
SEM MAG: 6.67 kx
Det: BSE, SE
View field: 41.5 µm
E7_1_2_a3
20 µm
MIRA3 TESCAN
Faculty of Engineering , CULS Prague

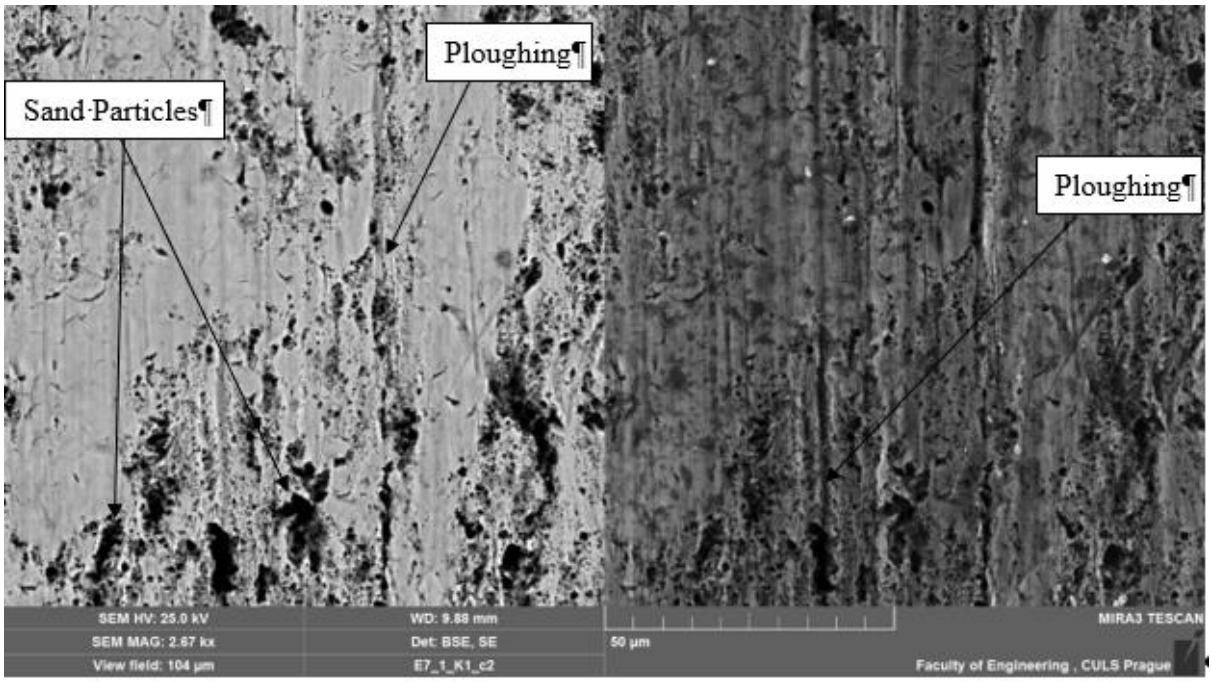
Ploughing¶
Sand·Particles¶
Ploughing¶
SEM HV: 25.0 kV
WD: 9.88 mm
MIRA3 TESCAN
SEM MAG: 2.67 kx
Det: BSE, SE
50 µm
View field: 104 µm
E7_1_K1_c2
Faculty of Engineering , CULS Prague

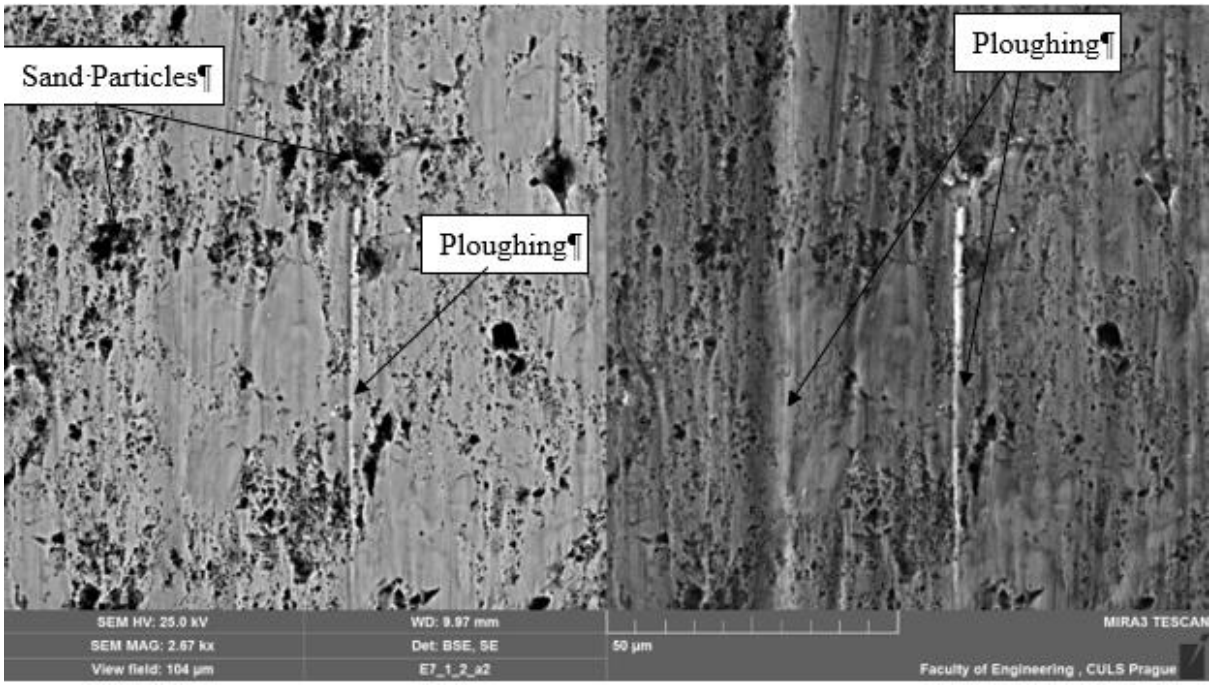
Sand·Particles¶
Ploughing¶
Ploughing¶
SEM HV: 25.0 kV
WD: 9.97 mm
MIRA3 TESCAN
SEM MAG: 2.67 kx
Det: BSE, SE
50 µm
View field: 104 µm
E7_1_2_a2
Faculty of Engineering , CULS Prague

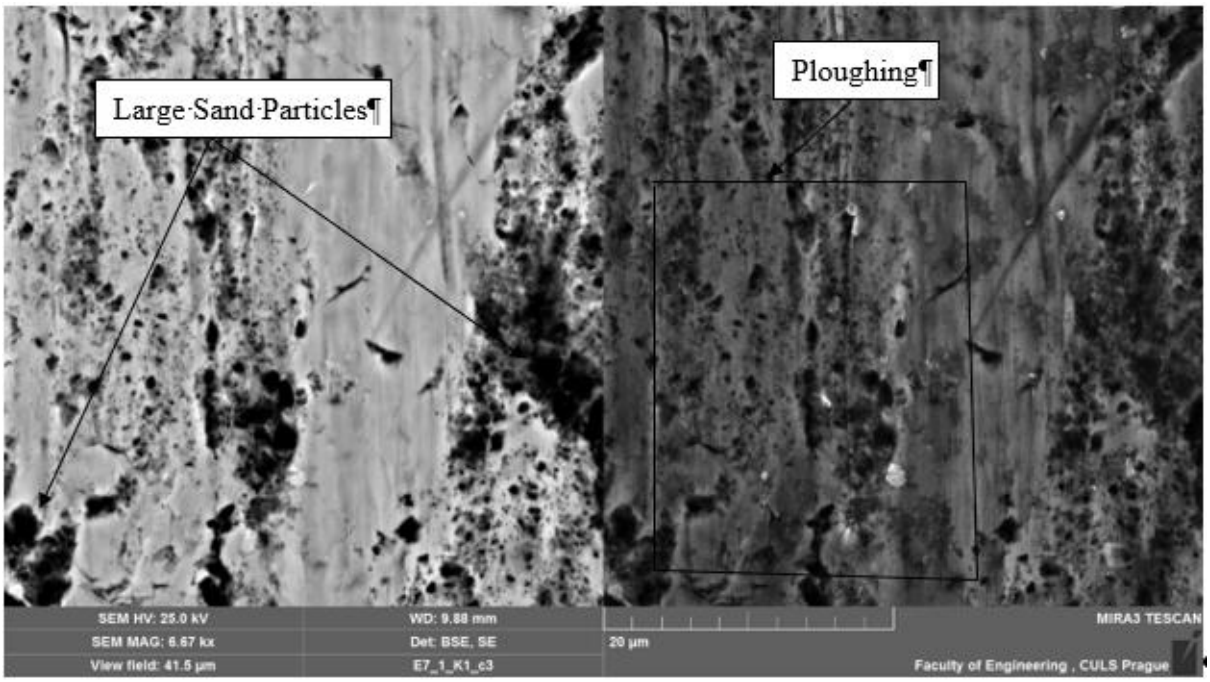
Large·Sand·Particles¶
Ploughing¶
SEM HV: 25.0 kV
WD: 9.88 mm
MIRA3 TESCAN
SEM MAG: 6.67 kx
Det: BSE, SE
20 µm
View field: 41.5 µm
E7_1_K1_c3
Faculty of Engineering , CULS Prague

APPENDIX 4

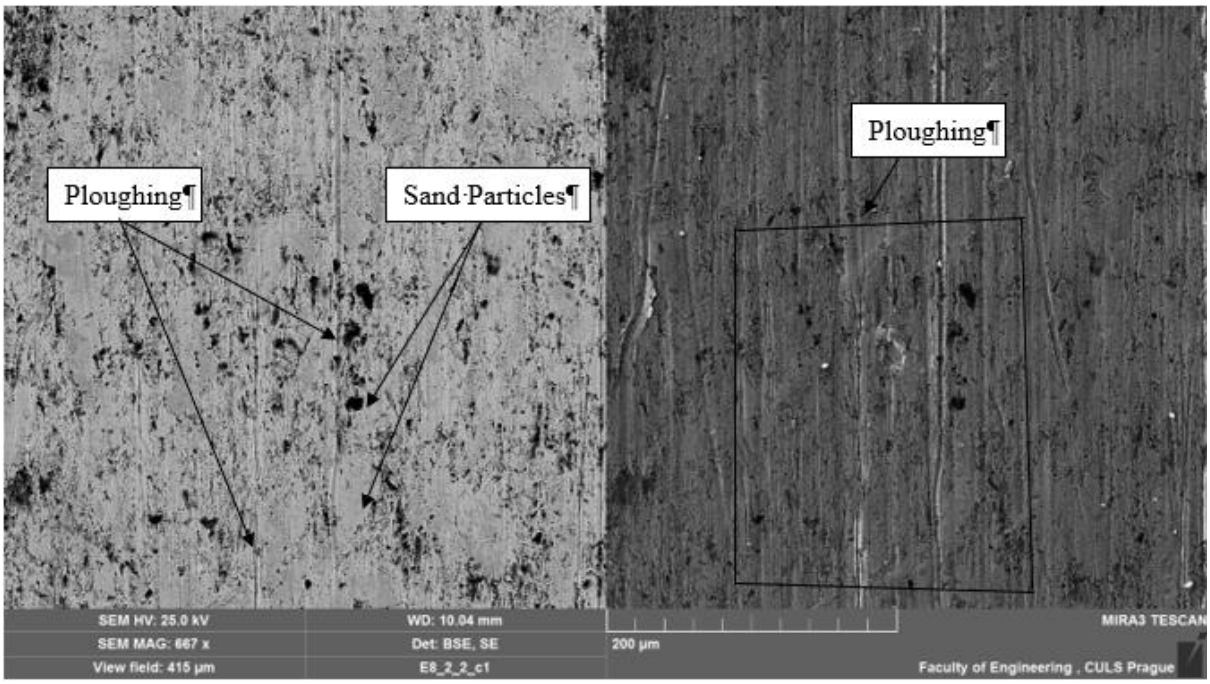
Ploughing¶
Sand·Particles¶
Ploughing¶
SEM HV: 25.0 kV
WD: 10.04 mm
MIRA3 TESCAN
SEM MAG: 667 x
Det: BSE, SE
200 µm
View field: 415 µm
E8_2_2_c1
Faculty of Engineering , CULS Prague

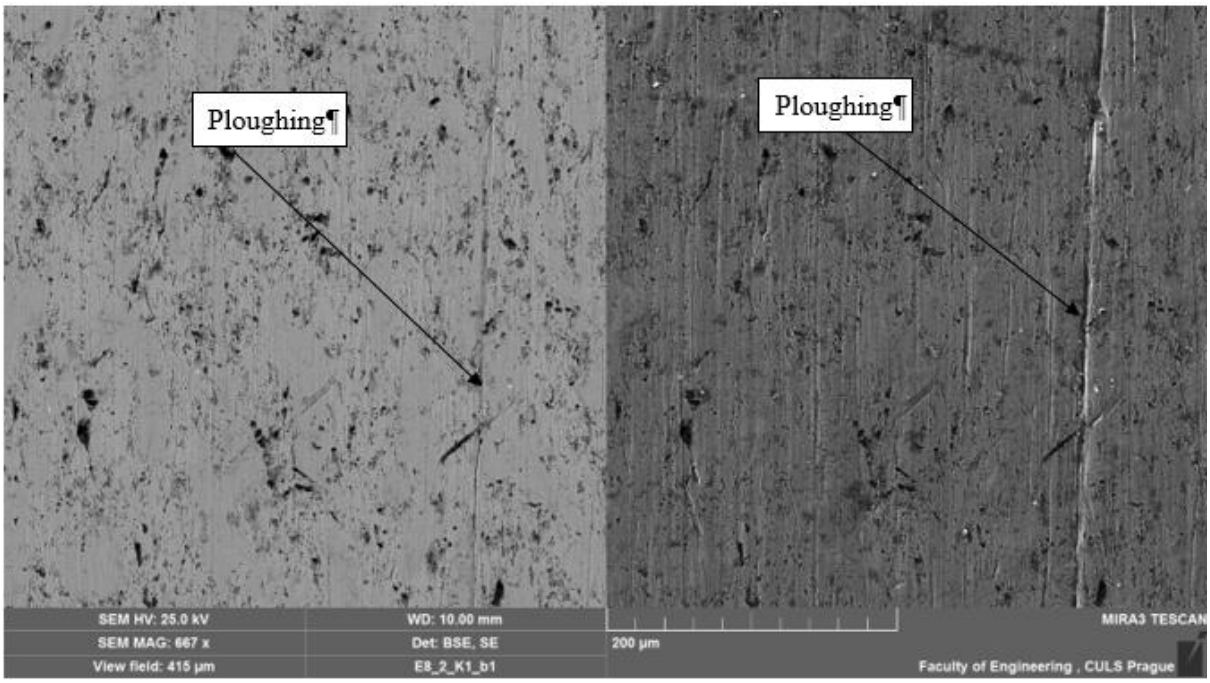
Ploughing¶
Ploughing¶
SEM HV: 25.0 kV
WD: 10.00 mm
MIRA3 TESCAN
SEM MAG: 667 x
Det: BSE, SE
200 µm
View field: 415 µm
E8_2_K1_b1
Faculty of Engineering , CULS Prague

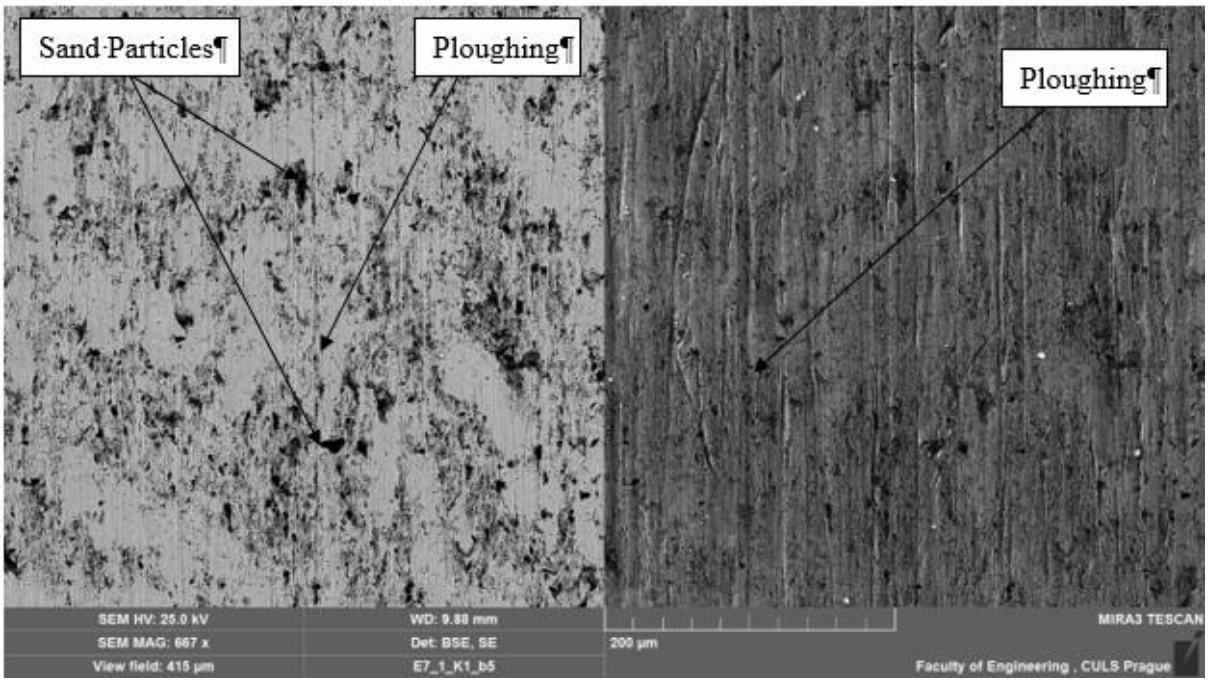
Sand·Particles¶
Ploughing¶
Ploughing¶
SEM HV: 25.0 kV
WD: 9.88 mm
MIRA3 TESCAN
SEM MAG: 667 x
Det: BSE, SE
200 µm
View field: 415 µm
E7_1_K1_b5
Faculty of Engineering , CULS Prague

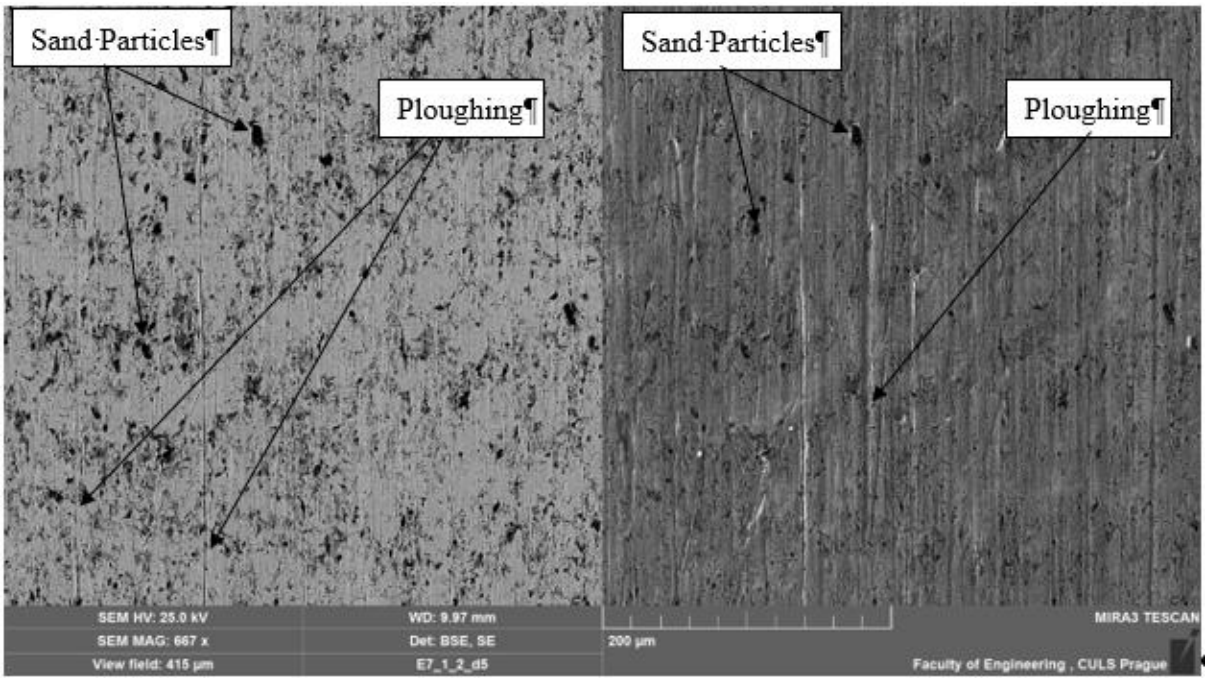
Sand·Particles¶
Ploughing¶
Sand·Particles¶
Ploughing¶
SEM HV: 25.0 kV
WD: 9.97 mm
MIRA3 TESCAN
SEM MAG: 667 x
Det: BSE, SE
200 µm
View field: 415 µm
E7_1_2_d5
Faculty of Engineering , CULS Prague

APPENDIX 5

Sample/mass (g)	0	210	420	630	840	1050	1260	1470	1680	1890
E82K1		0.01	0.0107	0.0099	0.0097	0.0109	0.0112	0.0097	0.0087	0.009
E71K1		0.0153	0.0162	0.0145	0.0135	0.0131	0.015	0.0127	0.0131	0.0129
E82K1S		0.0169	0.0136	0.0122	0.0127	0.0132	0.0133	0.0123	0.0137	0.0109
E71K1S		0.012	0.0113	0.0102	0.0108	0.0097	0.0111	0.0103	0.0094	0.0096

APPENDIX 6

Sample/cumulative (g)	0	210	420	630	840	1050	1260	1470	1680	1890
E82K1	0	0.01	0.0207	0.0306	0.0403	0.051	0.0624	0.0624	0.0808	0.0898
E71K1	0	0.0153	0.0315	0.046	0.0595	0.073	0.0876	0.1003	0.1134	0.1263
E82K1S	0	0.0169	0.0305	0.0427	0.0554	0.069	0.0819	0.0942	0.1079	0.1188
E71K1S	0	0.012	0.0233	0.0335	0.0443	0.054	0.0651	0.0754	0.0848	0.0944